GATING MECHANISM OF ATP RELEASE PANNEXIN CHANNELS

A dissertation

Presented to the Faculty of the Graduate School

of Cornell University

in Partial Fulfillment of the Requirements for the Degree of

Doctor of Philosophy

By

Erik Keone Henze

August 2022

GATING MECHANISM OF ATP RELEASE PANNEXIN CHANNELS

Erik Keone Henze, Ph.D

Cornell University 2022

Pannexins (Panx1-3) are members of the emerging large-pore channel family. Their ubiquitous expression and ability to permeate ATP or other small molecules has implicated pannexins, particularly Panx1, in a host of critical cell signaling roles. However, the stimulus which impinges upon pannexin itself to reversibly open the channel gate has remained elusive despite over 20 years of research into these enigmatic channels. Additionally, though there are over two dozen deposited structures obtained with various experimental manipulations, the molecular mechanism of pannexin channel gating is still largely unresolved.

We previously observed that pannexins can be activated by synthetic small molecules and hypothesized that pannexins may also be opened by naturally occurring small molecule ligands. Using a combination of patch clamp electrophysiology, chemical fractionation of mouse tissues, mass spectrometry, liposome reconstitution and a high-throughput screening assay, we found and defined a class of endogenous lipid molecules that function as bona fide agonists of Panx1 and Panx2. We also briefly explored phosphorylation as a gating stimulus for Panx1, which revealed a potential phosphoregulatory master switch for the channel in the distal N-terminus.

To better understand the gating mechanism, we used protein engineering and patch clamp to resolve a previously undefined domain in the Panx1 C-terminus that is essential for channel activation, which we dubbed the C-terminal activating domain (CAD). Integrating these findings with the available Panx1 structures offered a tentative basis for the first general Panx1

activation mechanism, wherein the CAD displaces the distal N-terminus by competing for a common binding site, leading to channel activation.

BIOGRAPHICAL SKETCH

Erik was raised on the Hawaiian island of Oahu where he developed a deep interest in the molecular basis of life, particularly in the context of cell signaling. After he acquired his BS in biochemistry and a minor in psychology from Hawaii Pacific University, he joined the Cornell field of biophysics to work under the guidance of Toshi Kawate.

Acknowledgements

My mother, brother and father have been a loving source of support and guidance. My mentor Toshi has been a constant catalyst for my growth as a scientist. He has also helped me to see my strengths and potential when I was doubtful of my ability to succeed. I am indebted to him, as well as the Cornell Molecular Medicine department for providing me a home to pursue my scientific goals. My friends Porter Hall and Brendan Ito have also been welcome companions during my time here in Ithaca.

TABLE OF CONTENTS

Introduction

The molecule ATP has a dual role; aside from being the primary molecule used by enzymes to catalyze chemical reactions, it exerts a wide range of autocrine and paracrine signaling effects upon its release from cells. In the extracellular space, ATP is progressively hydrolyzed to generate ADP, AMP, and adenosine by secreted and plasma membrane enzymes. The family of ionotropic (P2X) and metabotropic (P2Y) receptors known as purinoreceptors bind the purine ATP or its metabolite ADP. Another set of metabotropic receptors bind adenosine (AR). These receptors are widely expressed throughout the body, though in each cell type the expressed subset of P2X, P2Y and AR receptors varies considerably[1].

The ATP-gated P2X receptors are non-selective cation channels with substantial permeability to Ca^{2+2}. In the nervous system, they exert their effects on neuromodulation and synaptic transmission by membrane depolarization and through intracellular rises in the critical second messenger Ca^{2+3}. Outside of the nervous system, their signaling roles rely primarily on Ca^{2+} influx. The P2Y receptors are G-protein coupled receptors (GPCRs), which are stimulated in a subtype specific manner by either ATP, UTP, ADP or UDP[1]. They activate phospholipase C (PLC) or adenylate cyclase (AC) to generate the second messengers $DAG/IP_3/Ca^{2+}$ or cAMP, respectively[4]. The AR receptor family works through increases or decreases in the same set of second messengers, and the downstream consequences of this signaling generally oppose the physiological effects of P2X or P2Y receptor stimulation[5]. Thus, a negative feedback loop is built in to the purinergic signaling system through the opposing physiological effects of ATP/ADP and adenosine. The biological functions of purinergic signaling are manifold, but it is particularly important in the nervous, immune, and cardiovascular systems[1].

The trigger that initiates this suite of signaling is the regulated release of ATP into the extracellular space, which has been a subject of intense study over the past few decades. The two primary mechanisms involved are vesicular release and passive diffusion through ATP-

permeable ion channels[6–8]. The channels which are broadly responsible for this ATP release belong to an emerging family dubbed the ‘large-pore channels,’ which presently include connexin, innexin, LRRC8, CALHM and pannexin. In addition to their capacity for small-molecule flux, their subunits also share topological features such as cytoplasmic N and C-termini, 4 transmembrane helices, and two extracellular domains, which assemble into high oligomeric state (hexameric up to tridecameric) channels[8]. Excepting CALHM, they also share structural features such as the organization of their TM helix bundles and extracellular domains. Aside from their large pores, the most common structure-function relationship among the channels lies in their dynamic N-termini, which move within the pore or between the pore and cytoplasm. The N-termini contribute to functional properties such as channel gating, ionic selectivity and conductance[8].

Among these channels, pannexins are a three-member family (Panx1-3) which were discovered over 20 years ago. Noting that the gap junction channel family in vertebrates (connexins) and invertebrates (innexins) were not evolutionarily related, it was hypothesized that a common ancestor gap junction may yet exist. Pannexins were then discovered in vertebrates as modestly homologous to the invertebrate innexins[9]. Curiously, their biological role as a gap junction channel is still tentative. However, as an unopposed plasma membrane ATP channel with near ubiquitous expression[10–14], many autocrine and paracrine signaling roles have been established for pannexins, particularly Panx1.

Despite the plethora of assigned biological functions for the channel, comparatively little is known about its basic functional properties such as its channel gating mechanism and physiological gating stimulus. Indeed, even ATP permeability, pannexin's namesake property, appears to be dynamically regulated by presently unknown factors[15,16]. Pannexin biology is introduced below in the context of its most salient roles. This is followed by a critical discussion

on potential candidates for the channel gating stimulus and the major gaps in understanding of the channel gating mechanism.

Panx1 regulation of the inflammatory response

Purinergic signaling is critical for regulation of immune cell activation or suppression through stimulation of P2 receptors (ATP/ADP) or AR receptors (adenosine), respectively[17,18]. ATP and ADP function as damage-associated molecular patterns (DAMPs), which activate immune cells through their binding of various P2 receptors. This initiates, depending on the immune cell type, chemotaxis, proliferation, phagocytosis, release of cell-disrupting agents and/or secretion of cytokines to amplify the inflammatory response. AR receptor stimulation by adenosine generally opposes these processes. This has placed Panx1 at the heart of a delicate balance between the promotion and resolution of inflammation.

It was known that ATP release from apoptotic cells served as a 'find-me' signal to nearby immune cells, which induces chemotaxis towards the dying cell so that it can be phagocytized, and its contents recycled. After excluding vesicular release and connexin hemichannels, Panx1 was firmly established as the ATP conduit.[19] A general role for Panx1 in immune cell migration has since been elucidated by many studies showing that Panx1 is necessary for coordinated chemotaxis[18,20]. Interestingly, this is achieved both through autocrine signaling by Panx1 expressed on the migrating cells and paracrine Panx1 signaling to the migratory cells from the damaged, infected, or inflamed cells[21,22]. At the organismal level, endothelial Panx1 recruits and promotes invasion of circulating leukocytes into inflamed tissues[23]. In this capacity, Panx1 can serve an atheroprotective role. Macrophage recruitment to atherosclerotic lesions is a critical first step in the clearance of oxidized LDL particles (which generate a highly inflammatory milieu) by macrophage engulfment[24]. Indeed, KO of Panx1 in endothelial cell and macrophage precursor cells increases lesion size in mice models of atherosclerosis[25].

Panx1 can also function in an inflammation-resolving capacity. In mice models of asthma, adenosine generated downstream of Panx1-mediated ATP release suppresses $CD4^+$ effector T-cell activation, which tames the excessive inflammation asthmatics display in their lungs[26]. A retrospective analysis of human asthmatics found a decreased expression of Panx1 in peripheral blood mononuclear cells (PBMCs), which includes T-cells.

In different contexts, Panx1 promotes pathological outcomes due to pro-inflammatory signaling. Endothelial cell Panx1 increases the size of aortic aneurysms in mice through its ability to increase ATP release. This extracellular ATP recruits and activates macrophages, as well as induces inflammatory cytokine production, leading to pathological vascular remodelling[27]. A retrospective analysis found a lower incidence of aortic aneurysms in patients receiving the non-specific Panx1 inhibitors probenecid (for gout remedy) or spironolactone (for antihypertensive therapy).

Outside of apoptosis and asthma, the mechanism by which Panx1 activity is stimulated in these various contexts (aortic aneurysm models, cell infections or damage, etc) is largely unexplored.

Cardiovascular biology

Vasodilation and vasoconstriction are regulated through purinergic mechanisms. Broadly speaking, ATP release from the endothelium results in vasodilation while ATP release from smooth muscle results in vasoconstriction[28]. Panx1 contributes to both processes.

Adrenergic receptor stimulation induced vasoconstriction through vascular smooth muscle cells (VSMCs) by a purinergic signaling mechanism but at the time, the source of ATP release was not known[29]. A panel of Panx1 inhibitors and RNAi knockdown of Panx1 inhibited ~80% of phenylephrine (PE) – induced constriction of VSMCs, while overexpression of Panx1 enhanced vasoconstriction[29]. Importantly, vasoconstriction could be rescued by exogenous application of ATP to the VSMCs. Follow-up work showed that arterial blood pressure in freely moving mice

was reduced by conditional VSMC-specific knockout of Panx1[30]. The reduction occurred only at night, when the adrenergic system of mice (which are nocturnal) is most active. These and subsequent studies have elucidated the role of Panx1 as a major regulator of blood pressure[31–33], with translational human studies currently underway.

Mechanistically, increases in Panx1 channel activity occur downstream of adrenergic receptor stimulation by a Src kinase dependent mechanism involving phosphorylation at Panx1 residue Y199 (human numbering)[29,32,34]. At present, however, it is unclear if Y199 phosphorylation is required for Src to activate Panx1 through some other tyrosine, or if Src activates Panx1 through Y199 phosphorylation itself[35]. Thus, the mechanism of Src-mediated PE-induced Panx1 activation is uncertain.

Opposing VSMC vasoconstriction, Panx1 in the endothelium promotes vasodilation following adrenergic stimulation and shear-stress of arteries. In the case of PE-induced vasodilation, this occurs in areas where Panx1 is highly expressed in the endothelium but not smooth muscle[36]. Shear-stress induced ATP release through Panx1 causes relaxation in isolated arteries of mice[37,38]. At the organismal level, cerebral blood flow is altered and the vasodilatory response impaired in live mice with either P2 receptor or Panx1 KO[39].

The signaling pathway for endothelial Panx1-mediated vasodilation following PE stimulation have not been elucidated, though presumably it may share features with PE-induced vasoconstriction in smooth muscle. There is no mechanism proffered for Panx1 ATP release that mediated cerebral blood flow. Shear-stress induced Panx1 ATP release appears to be mediated through rises in intracellular Ca^{2+} following activation of the mechanosensitive cation channel Piezo1, which is discussed in further detail in the section on Panx1 mechanosensation.

Fat cell metabolism and body composition

Panx1 increases insulin-stimulated glucose uptake in adipocytes through ATP release[40]. Adipocyte-specific KO of Panx1 causes living mice to experience a larger and more sustained blood glucose level over time in response to a high glucose meal. The mice also displayed increased fat mass and decreased lean mass. These findings were replicated in another study of global Panx1 KO mice[41]. It was also found that obese human subjects had elevated levels of adipocyte Panx1. On the other hand, Panx1-mediated ATP release enhanced macrophage infiltration into adipocytes[42], which is a hallmark of the inflammation seen in obesity and diabetes. Additionally, global KO of Panx3 prevents a high fat mass, high-inflammation phenotype by reducing the total number of fat cells in mice[43], Thus, whether pannexins on the whole are protective, or whether they contribute to metabolic dysfunction in diabetes and obesity remains to be determined.

Mechanistically, Panx1 releases ATP in adipocytes following activation of protein kinase A (PKA) downstream of adrenergic receptor stimulation[42]. However, there are a large array of PKA effectors including other kinases, transcription factors, and lipases, so the gating stimulus of Panx1 in adipocytes remains to be determined.

Neuromodulation, learning and memory

Panx1 acts as a negative regulator of synaptogenesis during development and synaptogenesis in adult mice (reviewed in detail in[44]). Global Panx1 KO impairs short-term memory through the suppression of long-term depression (LTD), the weaking of synaptic connections[45]. Consistent with an inhibitory role at the synapse, another group reported that global KO of Panx1 increased dendritic spine formation in young mice[46]. This lead to a larger number of synaptic connections between different sets of neurons, known as network excitability. As in the above study, there was also increased levels of major excitatory signaling proteins (GluA1, GluN2, PSD-95) within synaptosomal preparations. It is speculated that this general inhibitory action of Panx1 is related

to its function as either a chloride channel or through the generation of adenosine following ATP release. No channel activation mechanisms have been offered for Panx1 in these studies.

Other biological roles

Many other isolated (patho)physiological roles for pannexins have been documented. For instance, multiple studies have shown that Panx1 deletion induces hearing loss in mice[47]. Panx3 plays a developmental role, as global Panx3 KO mice display decreases litter sizes and a higher rate of infant death[11]. Bone-specific KO of Panx3 causes small and improperly formed skeletal tissue[48]. Pathologically, Panx1 and Panx2 drive inflammation and cell death during ischemia reperfusion injuries[49]. Panx1 also contributes to the purinergically-mediated component of neuropathic and inflammatory pain[50].

What opens pannexin, and how does pannexin open and close?

As detailed above, there are many established and emerging biological roles of pannexin. Yet, there is comparatively little information to answer two of the most basic questions about any ion channel:

What is the biological stimulus received directly by pannexin which opens the channel?

Channel proteins are often classified by their natural gating stimulus, which may be voltage, small molecule ligands, mechanical forces, temperature, protons or other inorganic ions, or even light. To say that any one of these is a natural gating stimulus means that it physically interacts with the protein in such a way as to make an energetically favorable transition from a non-conducting (closed) state to a conducting (open) state. Typically, they act reversibly on time-scales characteristic of cell signaling (milliseconds to seconds) to trigger a biologically meaningful signal from the channel. A canonical example is the ligand-gated ion channel N-methyl D-aspartate receptor (NMDAR), which opens only when glutamate and glycine bind to their respective extracellular ligand-binding domains. Generally, a channel has one primary

stimulus class, though other stimuli, protein-protein interactions, or post-translational modifications may further enhance or suppress the channels activity. For instance, the pore of NMDARs opens once glutamate and glycine bind, but Mg^{2+} will bind and block the channel pore unless the membrane is simultaneously depolarized. In this way, removal of Mg^{2+} does not act as a gating stimulus per se, but is nevertheless necessary for NMDARs to fulfill their signaling role.

There are many reported ways to induce Panx1 channel currents, and essentially none for Panx2 and Panx3. For Panx1, these include voltage, mechanical forces, rises in extracellular K^+ or intracellular Ca^{2+}, addition or removal of various post-translational modifications, and removal of the distal C-terminus by caspase cleavage[15,16,51,52]. However, at present it is unclear if any of these act as a natural gating stimulus, in the canonical sense described above. The reasons for this relate to the lack of evidence for direct physical interaction or lack of control for other mediating factors, an unphysiological level of the stimulus required to open the channel, or no evidence of reversibility. This is detailed for each reported stimulus class below and where applicable, comparisons are made between Panx2 and Panx3 or other members of the large pore channel family.

Caspase cleavage

Panx1 is perhaps best known for its role in apoptosis, during which it is cleaved at its C-terminus by the proteases which execute the apoptotic process, known as caspases. The basally silent channel is irreversibly activated by this cleavage and leaks out ATP and other cellular metabolites, which recruit phagocytes to the dying cell and initiate inflammation-resolving cascades in the nearby cells[10,19]. It is clear that cleavage alone is sufficient to cause the channel to open, as genetic truncations at the caspase cleavage site can generate constitutively active channels in a variety of cell types[51,53–56]. Additionally, following reconstitution of purified Panx1 into liposomes or planar bilayers, caspase treatment generates

CBX-sensitive dye uptake and ionic currents[57,58]. Yet, caspase cleavage only occurs in cells undergoing apoptosis, and irreversibly opens the channel to an ATP-permeable state. This would be quite deleterious to a cell attempting to maintain metabolic homeostasis. The many roles of pannexins outside of apoptosis then indicate the existence of a different stimulus.

Voltage

Positive membrane potentials are universally accepted to stimulate Panx1 currents, and are the primary tool used to study Panx1 channel function via electrophysiology. The very first functional study of pannexins found that Panx1 (but not Panx2 or Panx3) generated outwardly rectifying currents when heterologously expressed in frog oocytes[59]. Though not stated explicitly, it is likely that voltage stimulation was tested because pannexin was thought to be a potentially new gap junction channel like connexins, which were already known to be voltage-gated channels[60]. The currents also displayed voltage-dependent kinetics (activation and deactivation), a characteristic sign of voltage gating. Follow-up studies with single-channel recordings demonstrated increases in Po with increasing membrane voltage[61–63]. However, the voltages need to effect a significant change are decidedly unphysiological. Indeed, the one study which completed a full voltage dose-response curve found an EV_{50} of about +40mV. This is out of the realm of what is experienced by most excitable cells, except in specific areas of neurons like the axon or dendritic arbors of pyramidal cells. Further, given pannexins function in many non-excitable cells (whose membrane potentials typically range from -70 to -20mV), the channel would never experience the potentials needed to stimulate its activity.

It should also be noted that the above studies were done using rodent Panx1 (either rat or mouse), which is spontaneously active (somewhat leaky, generates voltage activated currents, and some basal ATP release). In most mammalian cell studies, other Panx1 orthologous such as human Panx1 are basally silent. The reason for these species differences are not yet clear, though it may have something to do with propensity for different post-translational modifications

(discussed more in section below on PTMs). Finally, Panx2 also can generate outwardly rectifying currents similar to rodent Panx1[64,65].

Mechanical force

The second report of Panx1 channel function was motivated to find the channel responsible for initiating mechanically-stimulated calcium waves, which were known to be triggered by extracellular ATP. Given its association with the large pore gap junction channels, known hemichannel activity, and insensitivity to calcium (which silences connexin hemichannels), Panx1 seemed to be a prime candidate. They found that excised membrane patches from Panx1-expressing frog oocytes displayed a range of basal single-channel currents up to an extremely large conductance class of ~500pS[66]. Further, Po could be increased (~4-fold) by applying -40mbar, a level of mechanical stimulation routinely used in studies of other known mechanosensitive channels. They assessed ATP permeability by performing voltage ramps in solutions where, everything else fixed, ATP was swapped for chloride, and observed a shift in the reversal potential that was smaller than would be expected if ATP was completely impermeable to the channel. No inhibitors were used to confirm the channel identity, as little was known about its pharmacological profile at the time. A quick follow-up study identified Panx1 in erythrocytes by PCR and immunostaining, and found that hypotonic shock generated ATP release which could be blocked by CBX, an inhibitor of Panx1[67]. Importantly though, CBX also inhibits other connexins and many other channels capable of ATP release.

These two studies set the tone in the field that Panx1 is a mechanosensitive ATP release channel. Since then, many additional studies have found CBX-sensitive ATP release or dye uptake from various cell types following hypotonic shock, in some cases confirming Panx1-dependency through genetic addition (heterologous expression) or removal (knock-downs or KO) of Panx1. These studies are detailed further in other reviews[15,16]. However, there have been zero additional studies for the 20 years since the initial reports to provide further support

that Panx1 senses and responds to mechanical stimulation directly. This is an important distinction, as it has become clear that the primary mammalian mechanosensitive channel Piezo1[68], may be responsible for all findings of Panx1 mechanosensation at the cellular level. A series of studies have elucidated a Piezo1-Panx1 signaling complex, where the non-specific cation channel Piezo1 induces Panx1 ATP release by increasing cytosolic calcium[37,68–72]. One study found that the mechanism of Panx1 activation by intracellular calcium involves a CamKII-dependent phosphorylation in the distal C-terminus, S394[72].

In the absence of new evidence, the inherent mechanosensitivity of Panx1 remains to be demonstrated. However, innexin-dependent mechanosensitive currents have been observed in both *C.elegans* touch neurons and from heterologous expressed systems[73]. Further, innexin is required for mechanosensation in *C.elegans*, and can even imbue touch sensitivity in sensory organs not normally responsive to touch[74]. Crucially, in this same study, Panx1 expression rescued touch sensitivity in the innexin knockout worms. This suggests that Panx1 may be mechanosensitive after all. The field awaits functional data which conclusively demonstrate Panx1 mechanosensitivity.

Ions

Early functional studies of Panx1 reported that extracellular K^+ at 10mM and above caused a reversible increase in currents over the course of 5-10 minutes[75]. Follow up work by the same lab also showed that K^+ can increase Panx1 permeability to large anions and induce ATP release during voltage-clamp experiments, indicating it may trigger a large-pore conformation of the channel[56]. These are intriguing data, but the extracellular K^+ concentration required only occurs in certain pathological states such as anoxia. It also may not work directly. This is because treatment of Panx1 with K^+ induced no change in a high-resolution cryoEM structure[55]. Additionally, many groups have failed to find an increase in Panx1 currents by applying K^+[15,76–78].

Intracellular rises in Ca^{2+} also have been reported to induce Panx1 activity in excised membrane patches[79]. The data is not compelling, as all that is shown is one trace, where it is difficult to assess when and for how long Ca^{2+} was applied, or whether it was truly reversible. Also, like mechanical stimulation, this one report has not been repeated in over 15 years, and as with K^+, Ca^{2+} treatment failed to change the structure of Panx1 when applied directly[55]. Findings at the cellular level are confounded by the fact that Ca^{2+} stimulates Panx1 via CamKII phosphorylation, as described in the section on mechanosensation.

Post-translational modifications

The idea that post-translational modifications can act as a gating stimulus for pannexin comes from two different studies of phosphorylation and a recent study on acetylation. Initially, it was found that Panx1 activity increases following phosphorylation at Y199 by a Src family kinase downstream of adrenergic receptor stimulation.[30] Phosphorylation only 'tuned-up' activity (voltage activated currents, ATP release) of the already active mPanx1 channel by about 2-fold. However, follow-up work shows that the basally silent hPanx1 could generate sizeable voltage-activated currents following adrenergic receptor stimulation.[52] They refer to this conversion of the silent channel into a voltage-stimulated channel as 'activation.' Another group reported that Src kinase phosphorylation at Y309 was necessary for ischemia-induced Panx1-dependent currents in neurons,[80,81] though they never showed Panx1 opening due to Y309 phosphorylation in an isolated heterologous expression system.

The most compelling data for PTM stimulation of Panx1 comes from a recent study on deacetylation at residue K140. In this paper, inside-out patch clamp experiments demonstrate that simultaneous membrane depolarization and deacetylation of K140 causes Panx1 channels to open[52]. Further, when expressed in HEK293 cells, the deacetylation-mimicking point mutant K140R displayed robust voltage-activated whole-cell Panx1 currents.

The studies on phosphorylation and deacetylation provide some interesting clues on the regulatory mechanisms of Panx1. However, whether deacetylation or phosphorylation alone reversibly induce channel opening is still unclear. This is because voltage-stimulated currents were always used to assess changes in channel function between the different conditions in the study, and real-time reversibility of channel function by re-acetylation or dephosphorylation was not demonstrated.

An additional concern comes from considering the time scales involved in cycles of PTMs. The time scale of PTM cycling is generally longer (minutes) than the time scales which are typically associated with channel-based cell signaling. Thus, if a PTM left Panx1 channels open for minutes at a time, then the cell could lose appreciable amounts of ATP or other precious metabolites. Indeed, in WT HeLa cells, which express a small amount of endogenous Panx1, caspase cleavage of Panx1 can cause near total depletion of ATP in as little as 10 minutes, depending on the cell[82]. Over-expressing Panx1 caused every cell to lose its ATP in about 5 minutes. It is also telling that the first notion of Panx1 as a 'phosphorylation-gated channel' arose from a study showing that phosphorylation at residue Y309 was necessary to deliver the 'death-blow' to neurons challenged with ischemic conditions[80,81]. Nevertheless, it is possible that some Panx1-intrinsic or other cell based mechanism is able to suppress activity in a timely manner, or that the reverse PTM can occur quickly in specific signaling contexts.

An alternative interpretation of the literature is that certain PTMs are necessary to 'prime' pannexin to be able to respond to its natural gating stimulus. This is reflected in the fact that phosphorylated or deacetylated hPanx1 can generate sizeable voltage-activated currents, but the PTMs themselves do not generate large basal currents at resting membrane potential. The fact that cellular ATP release follows changes in PTM status may reflect the existence of a currently unknown gating stimulus present in tissues or cell culture conditions.

How does the channel open and shut to allow ion conduction?

The C-terminal pore plug mechanism has holes

Panx1 has a cytoplasmic C-terminus (residues 301-426). The Panx1 gating mechanism is currently thought to involve removal of the distal C-terminus out of the channel pore, which allows permeation of ions or small molecules. This arose out of a series of studies starting over 10 years ago. Prior to knowledge of Panx1 C-terminal caspase cleavage or structural data, a study sought to find Panx1 pore-lining residues using the cysteine accessibility method (SCAM). The SCAM results indicated that the distal C-terminus (residues 410-426) and TM1 may line the channel pore[83]. The same year, constitutive opening of Panx1 following C-terminal caspase cleavage (cleaves residues 379-426) was observed in apoptotic cells[19]. A follow-up study on the Panx1 activation mechanism by caspase found further support for a pore-associated distal C-terminus. Upon performing the substitution F53C (predicted to be near the extracellular side of TM1), Panx1 could not be activated by cleavage unless the cells were first pre-treated with the reducing agent DTT[53]. However, if the native residue C426 was concurrently substituted with serine (C426S/F53C), then cleavage activation proceeded as normal. This indicated that C426 may lie deep within the Panx1 pore, since C426 could be close enough to F53 to induce a disulfide bond. Since then, many papers have reported constitutive activity of Panx1 following genetic truncation to the caspase cleavage site[51,53–56].

The wealth of data supporting the C-terminal pore plug mechanism have been challenged, however, by structural and functional data reported within the last two years. Half a dozen different groups have deposited structures of the full-length channel, but the distal C-terminus (373 and on) was not resolved in any of them. One group claims to have located the C-terminus deep within the channel pore, but their CryoEM map is too low resolution in this region to confidently assign residue positions[84]. The density here may also be artificially produced by the use of symmetry operators during 3D reconstruction.

Additionally, two studies where a large portion of the C-terminus was removed (Δ356-426) paradoxically found that the channel is shut, as opposed to constitutively active. Importantly, like full length Panx1, the truncated constructs could still be activated by known hyperactivating modifications to the N-terminus[85], or downstream of adrenergic receptor stimulation[54]. The cytoplasmic domains in these structures also showed no structural difference compared to the full-length constructs. Furthermore, despite many structural studies, the C-terminal plug has not been revealed, and the channel can clearly shut or open independently of this region. These data cast doubt on the notion that the distal C-terminus acts as a simple plug.

The Panx1 N-terminus: An emerging role in channel gating

Panx1 has a short N-terminal domain (resides 1-31). A few years ago, our lab discovered that basally silent Panx1 can be activated by inserting the amino acids GS after the start methionine[63]. This serendipitous discovery (the insertion was in fact a cloning scar we previously overlooked) led to further observations that insertion of any hydrophobic amino acid at this position also activated the channel. This was followed by reports of an internal N-terminal deletion (Δ21-23) which activated the channel comparably to C-terminal truncation at the caspase cleavage site upon expression in frog oocytes and in HEK293 cells[55,86].

Panx1 structural data indicate that the most dynamic region of the channel (besides perhaps the distal C-terminus) is the N-terminus. Our structure of the C-terminally truncated Panx1 (Δ356-426) resolved the N-terminus extending into the cytoplasm[85]. On the other hand, a full-length structure showed the N-terminus folded up deep within the pore, towards the extracellular side of TM1[55]. Intriguingly, the point at which the N-terminus diverges between the structures lies at a pivot point comprised of amino acids 21-23, suggesting that this deletion can lock the channel in an activated state. Since then, out of the dozen or so different structures obtained, some show the N-terminus in the pore and others extended towards the cytoplasm. The experimental conditions between the studies varied too much to assess exactly what might be causing the

difference (insect cell vs mammalian cell protein expression, frog vs human Panx1 orthologue, truncated vs not truncated, detergent vs nanodisc reconstitution, etc).

One very recent study on the Panx1 inhibition mechanism has added some clarity. They found that the pore-associated N-terminus in their untreated structure relocated to its cytoplasmic binding pocket following treatment with the inhibitor probenecid[87]. Since all the experimental conditions were fixed, this conformational change was solely due to probenecid treatment. This indicates that the N-terminus flips down to inactivate or close the channel. If this is true, then an upward flip of the N-terminus should occur following treatment with a Panx1 activator.

A natural question at this point is whether C-terminal cleavage induces this flipped up N-terminus. The two groups that did resolve the N-terminus of the cleaved channel found it flipped up into the pore[55,87]. But their full-length structure also showed a flipped-up N-terminus, so it is hard to say if the C-terminal cleavage had any effect on the structure.

PTMs : How do these act on the channel?

Another question central to the Panx1 activation mechanism arises out of the fact that many different point mutations or modifications can activate the channel. Besides C-terminal cleavage, these include the distal N-terminus insertions, the ∆21-23 deletion, lysine deacetylation at K140, and phosphorylation at Y150 or Y199 or Y309 or S394. Additionally, the serine substitutions C40S and C347S also activate the channel[83,88]. Interestingly, a portion of these sites (K140, Y150, Y199, Y309 and C347) circumscribe the cytoplasmic N-terminal binding pocket. This suggests that perturbations to this region by the addition or removal of these PTMs may activate the channel by affecting the orientation of the N-terminus.

Finding the pannexin gating stimulus and resolving the Panx1 activation mechanism

My work has focused on finding a compelling natural gating stimulus for pannexins, and on the activation mechanism of Panx1. Towards finding the gating stimulus, we hypothesized that

pannexins may be opened by a yet-to-be discovered class of pannexin small molecule agonists (**Chapter 1**). This is because we previously observed that synthetic small molecules can open certain Panx1 when its putative pore-blocking site is removed[55,78,85]. To resolve the channel activation mechanism, I defined the region of the Panx1 C-terminus that is necessary for the channel to open following C-terminal cleavage (**Chapter 2**). I then assessed the relevance of this region for other Panx1 gating stimuli and related these findings to the emerging role of the N-terminus in channel gating. I also investigated the basis for Panx1 gating by phosphorylation (**Chapter 3**).

Chapter 1: Pannexins are lysolipid-gated ion channels

Introduction

Pannexins are a three-member (Panx1-3) family of ion channels broadly expressed throughout the body which mediate the cellular release of ATP and other small molecule messengers[10–14]. Their ability to promote small molecule release has implicated pannexins in many aspects of biology. Pannexin-mediated signals recruit cells to sites of inflammation and tissue damage[18,89], regulate blood pressure[32,38,90], act as neuromodulators[91] and effect cellular energy metabolism [40,92–94]. Pannexins also have many roles in promoting or abrogating pathological outcomes such as ischemic cell death[49,95], chronic pain[96], progression of atherosclerosis[25], and the metabolic dysfunction seen in diabetes[40,93,94]. The biochemical pathways that lead to the opening of pannexin channels have thus garnered great interest, to manipulate channel activity in the lab and the clinic.

During apoptosis the channel gate of Panx1 is irreversibly opened through caspase-mediated C-terminal cleavage, which is sufficient for the channel to fulfill its role as a conduit for the 'find-me' signals from a dying cell[10,19,58], But there are many signaling roles of pannexin in cells where no apoptotic program is active. In these instances, pannexin cargoes must be released in a regulated fashion to achieve cell signaling without significant depletion of precious cellular metabolites such as ATP. Yet at present it is unclear if any of the stimuli reported to open pannexin channels act as a physiologically relevant gating stimulus(reviewed in detail in[15,16]). These are principally positive membrane voltage, extracellular K^+, membrane stretch and cytoplasmic rises in calcium, which are reviewed in brief here.

Reversible, voltage-dependent opening of Panx1 has been reported[59,61–63], but only at positive membrane potentials that are not visited by most pannexin-expressing cells. Similarly, extracellular K^+ can open Panx1 but it requires pathologically high levels to effect channel

opening. It is also unclear if it works directly on the channel, due to a lack of any change seen in a K^+-treated high-resolution structure of Panx1[55], and the many groups unable to observe a modulatory effect of K^+ on Panx1 channel function[15,76–78]. Recent detailed studies involving pannexins role in mechanosensation now show it opens downstream of the bonafide mechanosensing channel piezo1 through intracellular signaling mechanisms[37,68–72]. In regards to Ca^{2+}, one initial study found evidence for a direct modulation of Panx1 channels, but follow-up work has failed to repeat this result[15,97], and as with K^+, no change in the high-resolution channel structure was observed upon treatment with Ca^{2+}[55]. Finally, phosphorylation, denitrosylation and deacetylation of key Panx1 cytoplasmic residues allow the channel to generate substantial voltage-activated currents, but by themselves have not been shown to open the channel[34,52,88]. Presumably then, these PTMs may prime the channel for opening by an as-of-yet unidentified signal. Thus, despite 2 decades of establishing the biological roles of pannexin, evidence for a physiological stimulus that directly and reversibly opens the channel remains scant.

We previously demonstrated that commonly used Panx1 inhibitors instead potentiate Panx1 when select point mutations are introduced to the channel[78]. Additionally, a recent structural study of Panx1 revealed a large conformational change following incubation with the inhibitor probenecid[87]. Together, these data demonstrate the existence of dedicated channel gating machinery which can be manipulated by small molecules to effect both channel opening and closure. This raises the possibility of naturally occurring small-molecule Pannexin agonists, which may serve a crucial regulatory role as a channel gating stimulus.

An unbiased screen of organic compounds extracted from mouse tissues revealed the first documented small-molecule that directly and reversibly opens Panx1 and Panx2: lysophosphatidylcholine (LPC). A CryoEM structure of the nanodisc-reconstituted Panx1 channel incubated with LPC revealed conformational changes which correspond to another recently proposed open state of the channel[87]. The major lysolipid-generating enzyme

phospholipase A2 (PLA2) was also capable of opening pannexins through hydrolysis of membrane lipids. Together, this establishes LPC as the first bona fide pannexin channel agonist.

Reagents

All detergents were purchased from Anatrace (Maumee, OH). All lipids were purchased from Avanti Polar Lipids (Birmingham, AL). Carbenoxolone (CBX), Arachidonic acid (AA), arachidonoylethanolamide (AEA), quercetin (QCT), chlorpromazine (CPZ), PP2, biotin and desthiobiotin and were purchased from Sigma-Aldrich (St. Louis, MO). Prostaglandins (PGE2, PGI2) were purchased from Abcam (Waltham, MA). Porcine pancreas sPLA2 (P6534) was purchased from Millipore Sigma (Burlingtom, MA). Z-DEVD-FMK (ZVAD, 210344-95-9) was purchased from Santa Cruz Biotechnology (Dallas, Tx). Mastoparan (MTP) was purchased from Santa Cruz Biotechnology (sc-200831) or Millipore Sigma (M5280). D-luciferin and luciferase were used from the Thermofisher (Waltham, MA) ATP determination kit (A22066). Lysolipids were dissolved in 100% $CHCl_3$ (Lysophosphatidylcholine (LPC) and Lysosphingomyelin (LSM)) or 70% EtOH-H_2O (Lysophosphatidylinonsitol (LPI), Lysophosphatidylethanolamine (LPE), and Lysophosphatidic acid (LPA)). Solvent was evaporated under a stream of N_2 and lipids stored at -20C. On the day of experiments, lipids were redissolved in EtOH (LPC, LSM) or 70% EtOH-H_2O (LPI, LPE, LPA) and then diluted into the indicated buffer.

Generation of expression constructs

DNA constructs corresponding to the amino acid sequences of hPanx1 (NP_056183.2), frPanx1 (NP_001123728.1), hPanx2 (NP_443071.2) and hPanx3 (NP_443191.1) were synthesized by GenScript. A plasmid encoding mVenus (AAZ65844.1) was a kind gift from Matthew Paszek (Cornell University). Two point mutations (H148Q and I152L) were then introduced which enhance the ability of iodide to quench mVenus fluorescence[98]. For transient transfections, all

constructs were subcloned into a pIE2 plasmid backbone as previously described[63,78]. Constructs did not contain an affinity tag or N-terminal modifications/insertions unless otherwise specified.

The construct for baculoviral expression and purification of frPanx1 ΔLC (+GS) in insect cells was generated and subcloned into pCNG-FB7 Fastbac vectors as described previously[85]. For baculoviral expression in mammalian cells, the MCS of the pEZT-BM Bacmam plasmid (addgene:74099) was modified to contain an open-reading frame with internal BamHI and XhoI restriction sites. All pannexin constructs were subcloned into the BamHI/XhoI site, resulting in an N-terminal Gly-Ser and C-terminal Ala-Ser-Ser insertion. The N-terminal Gly-Ser was removed by PCR. For purification of hPanx1 from HEK293 GnTI- cells, intracellular loop residues 175-182 were replaced with a StrepII tag. For experiments involving co-expression of mVenus, the pEZT-BM plasmid was further modified by insertion of an EMCV IRES site after the open reading frame, followed by a second open-reading frame with AgeI/NotI restriction sites, into which mVenus was subcloned. All PCRs to introduce point mutations or remove amino acid insertions were performed using the Agilent (Santa Clara, CA) Quikchange II PCR kit. Overhang extension PCR to exchange amino acids or subclone constructs was performed using the Agilent Herculase II kit. All constructs were verified by sanger sequencing.

Cell culture

HEK293 (CRL-1573) and HEK293S GnTI- (CRL-3022) cell lines were purchased from the American Type Culture Collection and therefore were not further authenticated. The mycoplasma contamination test was confirmed to be negative at the American Type Culture Collection. HEK293 cells were maintained in Dulbecco's modified Eagle medium (Gibco) supplemented with 10% FBS (Atlanta Biologicals) and 10 µg/ml gentamicin (Quality Biological). HEK293 GnTI- cells were maintained in FreeStyle 293 (Gibco) supplemented with 2.5% FBS at a shaking speed of 125rpm. HEK cells were kept at 37°C with 8% CO2 in a humidified

incubator. Sf9 cells (GibcoTM, CN: 11496015) were maintained in Sf-900 III SFM (Gibco, CN: 12658019) and High five cells (Gibco, CN: B85502) cells were maintained in ESF 921 (Expression systems, Item: 96-001-01). Both insect cell lines were grown at 27°C and a shaking speed of 125rpm.

Baculovirus Production

Baculovirus production for mammalian cell expression was adapted from a previous protocol[99,100]. Fast-bac and Bacmam expression constructs were transformed into DH10bac cells. Bacmid DNA was isolated from positive colonies grown overnight in liquid culture. Using PEI, bacmids were then transfected into sf9 cells ($8x10^5$ cells/well) dispensed in a 6-well plate. Seven to eight days later, P1 virus was harvested and stored at 4°C. To generate P2 virus, sf9 cells ($1x10^6$ cells/mL) were infected with P1 virus at a 1000:1 (v/v) ratio. The P2 virus was harvested 3.5-4 days later and stored at 4°C.

Electrophysiology

HEK293 cells (passage no. 4–40) or HEK293 GnTI- (passage no. 4-40) were plated at low density onto 12-mm glass coverslips (VWR) in wells of a six-well plate (Greiner). Cells were transfected after 24 h with ~700 ng plasmid DNA using FuGENE6 (Promega) according to the manufacturer's instructions, or infected with 5% (V/V) bacmam P2 virus. For all other constructs, recordings were obtained 40-60hrs after infection/transfection. Borosilicate glass pipettes (Harvard Apparatus) were pulled and heat polished to a final resistance of 2-4 MΩ and backfilled with (mM) 147 NaCl, 10 EGTA, and 10 HEPES (adjusted to pH 7.0 with NaOH). Patches were obtained in an external buffer containing (mM) 147 NaCl, 2 KCl, 2 $CaCl_2$, 1 $MgCl_2$, 13 glucose, and 10 HEPES (adjusted to pH 7.3 with NaOH). For ionic selectivity experiments, NaCl was replaced with equimolar NaGluc or NMDGCl in both external and pipette buffers. A rapid solution exchange system (RSC-200; Bio-Logic) was used for recordings in which patches

were perfused with drugs or mouse fractions. Currents were recorded using an Axopatch 200B patch-clamp amplifier (Axon Instruments), filtered at 2 kHz (Frequency Devices), digitized with a Digidata 1440A (Axon Instruments) with a sampling frequency of 10 kHz, and analyzed using the pCLAMP 10.5 software (Axon Instruments).

Activity-guided fractionation of rat livers

A 10 g sample of frozen mouse livers was extracted in 100 mL 80% MeOH in water with dry ice via laboratory blender. The resulting suspension was sonicated with a microtip probe sonicator (Qsonica Ultrasonic Processor, Model Q700) for 2 minutes, 100% power, 50% duty cycle, with the sample in an ice bath. Following sonication the suspension was centrifuged at 5250 G at -10 °C for 20 min and the supernatant concentrated *in vacuo* with a Speedvac Vacuum Concentrator (ThermoFisher), loaded onto 2 g Celite, and fractionated by medium pressure reverse-phase chromatography (30 g C18 Combiflash RediSep Gold column). An aqueous acetonitrile solvent gradient was used at a flow rate of 40 mL/min, starting at 5% acetonitrile for 5 min and increasing to 100% acetonitrile over a period of 1 hr. The resulting 133 fractions (18 mL each) were pooled to yield 19 fractions, and the solvent removed *in vacuo*. The resulting residues were resuspended in 300 µL aqueous DMSO, ranging from 25% DMSO for fraction 1 and increasing by 5% for each successive fraction. The fractions were diluted 20-fold with patch clamp external buffer prior to assaying.

100-gram fractionation and re-fractionation

Extraction and the initial fractionation was performed as described above, using 300mL 80% MeOH for extraction. Fractionation was performed over a 240g RediSep C18 column, with a flow rate of 125mL/min. The resulting 196 fractions (24mL each) were once again combined to generate 19 pooled fractions. From these, fractions 11 and 12 were combined for re-fractionation by preparative reverse-phase UHPLC using a Thermo Hypersil GOLD C18 column

(10×200 mm 5 µm particle diameter) and 0.1% aqueous formic acid-acetonitrile gradient at a flow rate of 5 mL/min. The resulting 25 fractions were combined to generate 9 pooled fractions. The resulting material was resuspended in 400uL of DMSO and stored at -20C. Samples were diluted 300-fold into patch clamp external buffer on the day of recording.

UHPLC-HRMS

Liquid chromatography was performed on a Thermo Vanquish Horizon HUPLC coupled with a Thermo Q-Exactive HF high-resolution mass spectrometer. UHPLC separation was achieved using a Thermo Hypersil GOLD C18 column (2.1×150 mm 1.9 µm partical size) maintained at 40 °C. Normal chromatographic conditions began with an isocratic gradient of 99% water with 0.1% formic acid and 1% acetonitrile with 0.1% formic acid until 3 minutes, followed by a linear ramp to 98% acetonitrile at 20 minutes which was held for 5 minutes.

Feature Analysis

UHPLC-HRMS data were analyzed using Metaboseek software after file conversion to the mzXML format via MSConvert (version 3.0, ProteoWizard)[101,102]. The feature filtration criteria used were a minimum 3-fold increase in the most active fractions, fractions 7 and 8, over the neighboring fractions 6 and 9 and a minimum intensity of 100,000 for the feature of interest in the active fractions. The resulting features were manually curated to remove isotopes, adducts, and fragments, yielding eight metabolites of interest. MS2 analysis identified three of the compounds as pairs of isomers for lysophosphatidylcholine 16:0 and lysophosphatidylcholine 22:5 while the remaining five are at present unidentified.

Cell surface biotinylation

HEK293 or HEK293 GnTI- cells were dispensed into a 6-well plate. At 80% confluency, cells were transfected using JetPrime (Polyplus) according to manufacturer's instructions with 2.5ug of FLAG-tagged pIE2-pannexin constructs. Panx1 and Panx2 were C-terminally tagged and

Panx3 was N-terminally tagged. To match approximate transfection efficiencies, HEK293 GnTI- cells were transfected with half the amount of transfection mixture. Two days post-transfection, cells were transferred to a microcentrifuge tube and washed 2x in ice-cold PBS. Cell surface biotinylation, pulldown and subsequent immunoblotting were performed as described previously[78]. For the anti-FLAG immunoblots, two and three-fold more Panx2 and Panx3 samples were loaded relative to Panx1.

Panx1 expression and purification from High five cells and GnTI- cells

High five insect cells (3.5 x 10^6 cells/mL) were infected with 1% v/v P2 virus and 48 hours later, harvested by centrifugation and washed once with PBS. Nitrogen cavitation (4635 cell disruption vessel; Parr Instruments) at 750 psi was used to lyse the cells in PBS buffer supplemented with a PI cocktail (2.0 µg/mL leupeptin, 8.0 µg/mL aprotinin, 2.0 µg/mL pepstatin and 0.5mM phenylmethylsulfonyl fluoride). Cell debris was collected with a 12,000g spin for 10 minutes, and membranes were pelleted from the resulting supernatant by ultracentrifugation at 185,000g for 45 minutes. Membranes were flash frozen in liquid N_2 and stored at -80C. Membranes were thawed on ice, dounce homogenized then transferred to S buffer (1X PBS, PI cocktail, 10% glycerol and 1% C12E8) and mixed for 60 minutes. Following ultracentrifugation at 185,000g for 45 minutes, the supernatant was diluted 4-fold in PBS and incubated with StrepTactin Sepharose resin (Cytiva, PN: 28935600) for 60 minutes in batch. Resin was loaded on a gravity column and washed with 10 column volumes of wash buffer (150 mM NaCl, 100 mM Tris-HCl pH 8.0, 10% glycerol, 0.27% C12E8) and eluted with 5 column volumes of wash buffer containing 2.5mM desthiobiotin. Protein was concentrated and further isolated by size-exclusion chromatography (Superdex 200, PN: 28990944) in SEC buffer (150mM NaCl, 20mM Tris-HCl pH 8.0, 0.27% C12E8). The resulting peak fractions were used for liposome assays or structural studies. All steps were carried out at 4°C or on ice.

GnTI- cells (3.5 x 10^6 cells/mL) were infected with 10% v/v P2 virus and supplemented with 5mM sodium butyrate 12 hours later. Cells were harvested 60 hours post-infection by centrifugation, washed once with PBS, then solubilized in S buffer for 60 minutes. The sample was centrifuged at 5,000g for 10minutes then the supernatant was centrifuged again at 185,000g for 45 minutes. Panx1 protein was purified from the supernatant with Strep-Tactin XT resin (Cytiva, PN: 29401326) as described above, using 25mM biotin instead of 2.5mM desthiobiotin for elution. SEC was also performed as described above. All steps were carried out at 4°C or on ice.

Cellular mVenus quench assay

HEK293 or HEK293 GnTI- cells were dispensed into 96-well Poly-D-Lysine coated, black-walled plates. At ~90% confluency, cells were infected with 10% (v/v) P2 virus and 10-12hrs after infection, supplemented with 5mM (final concentration) sodium butyrate. The quench assay was performed 40-48 hrs after infection, except experiments involving hPanx1 expressed in HEK293 GnTI-, for which the assay was performed 36-40hrs after infection. Following infection, growth media was replaced with NaI buffer containing (mM) 147 NaI, 2 $CaCl_2$, 2 KCl, 1 $MgCl_2$, 10 HEPES, 13 Glucose, pH 7.3. For experiments involving LPA, a modified Ca^{2+}-free buffer was used to prevent precipitation of LPA: (mM) 147 NaI, 2 KCl, 1 EGTA, 10 HEPES, 13 Glucose, pH 7.3. Cells were equilibrated in NaI buffer for 10 minutes. All compounds specified as pre-incubated were added during this period. Activators and/or inhibitors were then added, and the fluorescent signal (Ex: 480/20, Em: 528/20) was monitored with a Biotek Synergy2 plate reader for 10 minutes. Finally, 1% (v/v, final) Tween-20 was added and fluorescence monitored for an additional 3 minutes to obtain the maximum quenching signal. The percent of quenching Q(t) was calculated according to the following formula: $Q(t) = 100 * \frac{F(t) - F_i}{F_f - F_i}$

Where F_i is the initial fluorescence value of the 10-minute read, F_f is the final fluorescence value following addition of 1% Tween-20, and F(t) the fluorescence value at each time point. Each condition was tested in experimental triplicate and the resulting averaged Q(t) was used to obtain quenching rates in the initial linear range using the SLOPE function in Microsoft Excel. In the dot-plots, each displayed data point represents the initial rate from a single triplicate-averaged trial. The points displayed in each dose-response plot are the average of at least 4 individual triplicate-averaged trials. To obtain fit parameters for the dose-response curves, the initial quenching rate in cells expressing mVenus only was subtracted from the initial rate obtained from cells expressing mVenus + pannexin for each concentration of lysolipid. These background-corrected dose-response plots were then fit to the Hill equation in mathematica to obtain EC50, the hill coefficient (n) and the maximum quenching rate (m).

Panx1 proteoliposome YOPRO uptake assay

DNA-incorporated proteoliposomes were prepared essentially as described previously[103]. Briefly, lipids prepared in chloroform were added to a glass tube and solvent evaporated under N_2. Lipids were redissolved in pentane and dried again under N_2, then resuspended in liposome reconstitution buffer ((mM) 50 Tris-HCl, 150 NaCl, 0.1 EGTA, pH 7.4)) to a concentration of 10mg/mL using bath sonication. Liposomes were freeze-thawed in liquid N_2 twice and stored at -80C. Thawed liposomes were extruded thirteen times through a 400nm polycarbonate filter, incubated with 0.65% (w/v) DDM for 15 minutes at RT, then incubated with pannexin protein in a 50:1 (w/w, hPanx1 SS4) or 100:1 (w/w, frPanx1 ΔLC +GS) ratio for an additional 30 minutes at RT. Detergent was removed from the mixture by four rounds of incubation with fresh 50mg Bio-beads SM2: twice for 60 minutes at RT, once at O/N at 4°C and once more for 60 minutes at RT. After Bio-bead removal, proteoliposomes were mixed with a complementary 20bp pair of primers (40uM each) and subjected to three freeze-thaw cycles in liquid N_2, then extruded through a 200nm polycarbonate filter. Unincorporated DNA was digested by incubation with

0.2mg/mL DNAse + 5mM $MgCl_2$ for 60 minutes at RT, then washed away by twice pelleting liposomes (280,000g for 20min at 4°C) and resuspending in liposome reconstitution buffer. DNA-incorporated proteoliposomes were pelleted once more, then resuspended to a final concentration of 10mg/mL. Liposomes were stored at 4°C and used within 48 hours.

100ug of proteoliposomes were dispensed into 96-well Poly-D-lysine coated black-walled plates (Corning, CN: 3372). With the Biotek Synergy2 plate reader, baseline fluorescence was read for 3 minutes, then 60nM YO-PRO-1 iodide (Thermofisher, PN: Y3603) and the indicated activators/inhibitors were added. Triton-X100 (1% v/v) was added to each well to obtain the maximum YOPRO signal. Data were normalized using the formula described for the cellular mVenus quench assay.

Cellular ATP Release Assay

Cells were prepared as described for the mVenus assay, using Costar 96 well white-walled plates (Corning, PN: 3610) coated with Poly-D-lysine (Gibco, PN: A3890401) according to manufacturer's instructions. Cells were washed once with NaCl external patch clamp buffer, then incubated in external buffer containing D-luciferin (0.5mM) and luciferase (1.3ug/mL) for 10minutes. LPC 16:0 (30uM) and/or CBX (50uM) were added, and the luminescence at 10minutes was measured using the Biotek Synergy2 plate reader. To control for initial cellular ATP content, luminescence was normalized to the value obtained following addition 1% Triton-X100 to buffer-only treated cells prepared on the same day.

Results

LPC is a naturally occurring pannexin-1 and pannexin-2 agonist

We searched for naturally occurring pannexin agonists in mouse tissues. Briefly, an organic extract of mouse liver was subjected to polarity-based fractionation, and the resulting fractions were tested for their ability to generate reversible, pannexin-dependent currents via whole-cell patch clamp (Figure 1). To increase the sensitivity of our screen, we used a hyperactive version of Pannexin-1 we previously reported (Panx1 +GS)[63]. We also tested pannexin-2, as it has been shown to form functional voltage-activated plasma membrane ion channels by whole-cell patch clamp[64,65]. We did not use pannexin-3 because it has not been shown to generate ionic currents

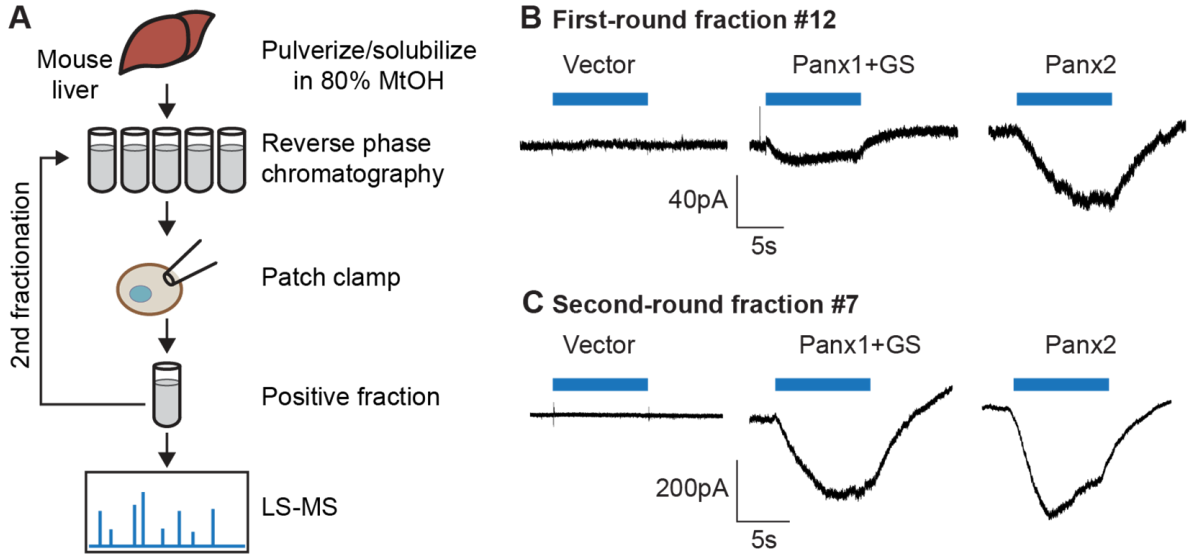

Figure 1. Activity guided fractionation to search for pannexin agonists **(A)** Schematic of screening process. Mouse livers were blended in methanol (MtOH), subjected to polarity-based fractionation, and assessed for their ability to stimulate currents in HEK293 cells expressing the indicated construct using whole-cell patch clamp. Fractions which induced this current were re-fractionated, reassessed by patch clamp, and the new active fractions analyzed for small molecule content by LC-MS. **(B)** Representative patch clamp traces from the first round and **(C)** second round. Blue bars indicate application of fractions.

in patch clamp experiments. Upon application of fraction 12 and to a lesser extent fraction 11, we found modest pannexin-dependent increases in whole-cell currents which reversed upon washout (Figure 1, Figure 2A,B).

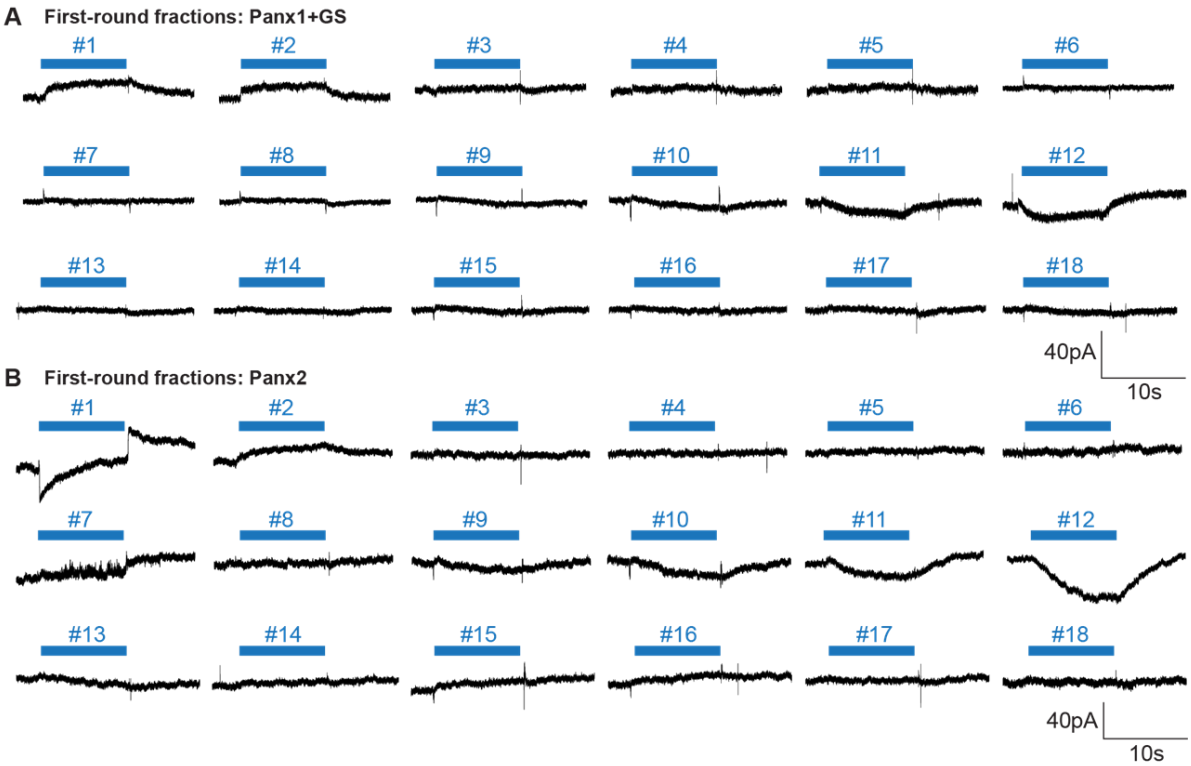

Figure 2. Activity of all first-round fractions tested by whole-cell patch clamp. **(A, B)** Representative traces of first-round fractions. Note that fraction #1 could produce currents in vector-transfected cells (not shown), and this current appears in (B).

We then combined 11 and 12 to generate a new set of 9 fractions. From these, we recovered robust pannexin-dependent currents in fractions 7 and 8 (Figure 2 continued, C,D,E). Mass spectrometry analysis of fraction 7 and 8 identified two lysophosphatidylcholine (LPC) species and their respective isomers, which were enriched in fractions 7 and 8 when compared to the neighboring fractions 6 and 9. Accordingly, we assessed the ability of pure LPC to open pannexin channels, focusing on the biologically predominate form identified in our analysis[104], LPC 16:0 (Figure 3). Pure LPC 16:0 induced a reversible current in HEK293 cells expressing hPanx1(+GS) or Pannexin-2, but not Pannexin-3 or a GFP-control (Figure 3). The size of the LPC-induced currents were comparable to those generated by fractions 7 and 8. Further, the concentration of total LPC 16:0 within the most active fraction 7 (19.7 ± 0.2uM) was estimated to be within 3-fold of the pure LPC 16:0 (7uM) species used in our whole-cell patch clamp experiments. These data demonstrate that the LPC 16:0 content of 7 and 8 is sufficient to

generate the pannexin-mediated ionic currents induced by application of these fractions. Finally, application of carbenoxolone (CBX), which inhibits Panx1 but not Panx2,[65] only inhibited LPC currents in cells expressing Panx1 channels (Figure 3B). This confirms that pannexins themselves are the carriers of the LPC generated currents.

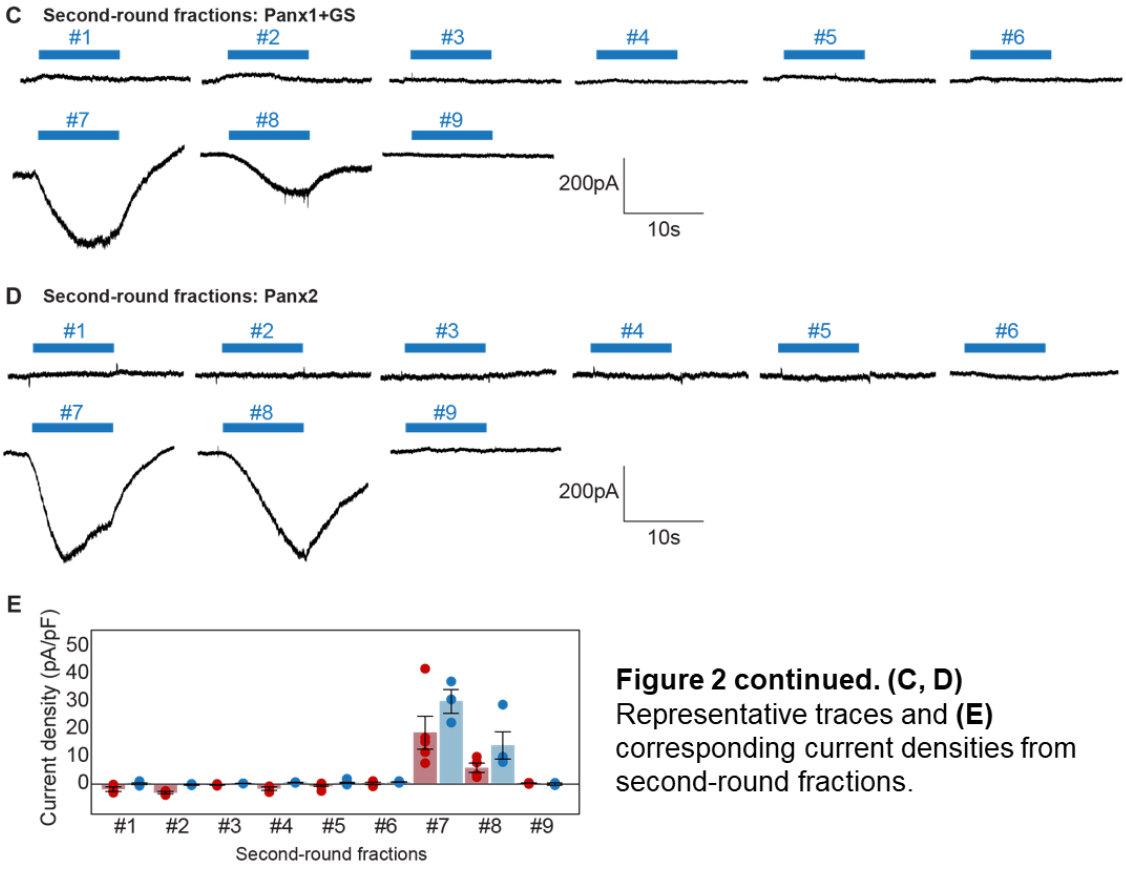

Figure 2 continued. (C, D) Representative traces and **(E)** corresponding current densities from second-round fractions.

The wild-type hPanx1 channel was not opened by LPC in HEK293 cells. However, LPC opened Panx1 when it was expressed in an alternate cell line commonly used for heterologous protein expression, HEK293S GnTI^{-}. Pannexin2 and Pannexin3 responses to LPC were the same in

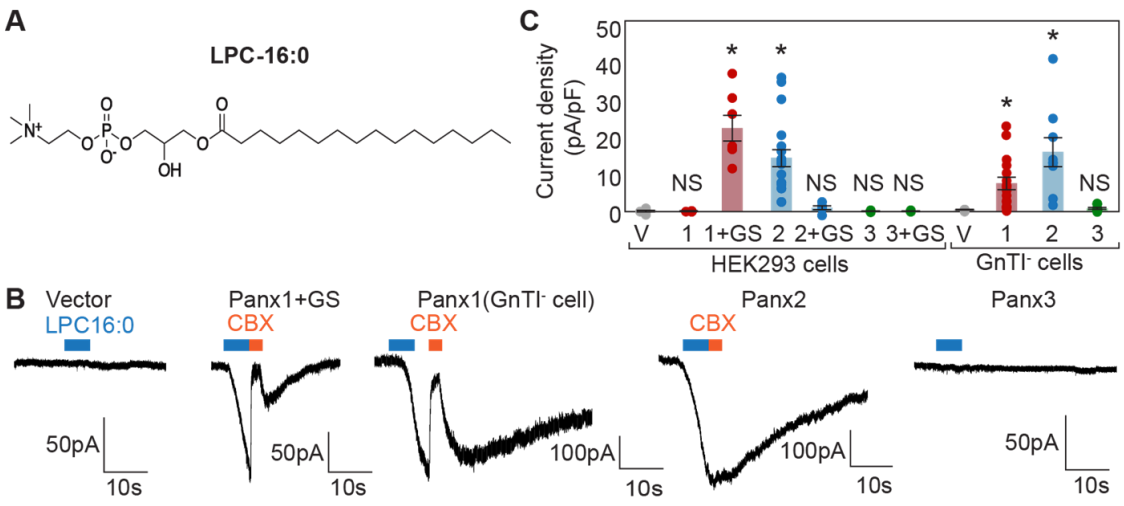

Figure 3. Mass-spectometry reveals the pannexin agonist LPC-16:0. **(A)** Skeletal structure of the enriched compound in fractions 7 and 8 identified via metaboseek, LPC-16:0. **(B)** Exemplar patch clamp traces of LPC-16:0 (7uM) to pannexin or vector only expressing cells. Red bars denote application of CBX (50uM). **(C)** Current densities obtained from applying LPC-16:0 to HEK293 or GnTI- cells expressing the indicated construct. Asterisks denote statistical significance with respect to the respective vector conditions.

HEK293 and GnTI-. Assessing cell-surface expression revealed an increase (~3 fold) surface expression of Panx1 and Panx2 subtypes in GnTI- cells compared to adherent 293 (Figure 4). While this could enhance whole-cell pannexin currents from GnTI in general, it is unlikely to account for the all-or-nothing difference between GnTI and 293 unique to Panx1. A change in Panx1 protein-protein interactions or PTMs between these two cell types may instead be responsible for the difference in channel function. Whatever the reason for this difference in

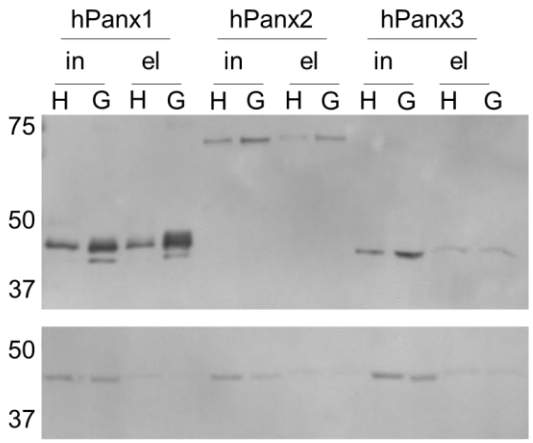

Figure 4. Cell-surface expression of pannexin is higher in GnTI- cells. Cell surface biotinylation pulldown of HEK293 (H) or HEK293 GnTI- (G) expressing the indicated FLAG-tagged pannexin construct. The total input protein to pulldown (in) and the surface protein isolated by pulldown (el) are compared between each cell line.

function, GnTI- cells afforded the ability to study lysolipid activation of the wild-type hPanx1. We therefore used GnTI- cells to study Panx1 and continued our use of HEK293 cells to study Panx2.

Different modes of stimulation have been reported to generate Panx1 channels with different ionic selectivity[15,16]. We therefore established the permselectivity of LPC-gated pannexin currents. Substitution of Cl^- with $Gluc^-$ in both pipette and extracellular buffers ablated LPC currents, while substituting Na^+ with $NMDG^+$ produced only a small reduction in currents. These results indicate a substantial preference for anions over cations, which is in general agreement with the reported selectivity of Panx1 stimulated by positive voltage or C-terminal cleavage[56,61,105]. We also assessed the ability of Panx1 and Panx2 to release ATP in response to LPC stimulation. We found that LPC caused a CBX-sensitive release of ATP from Panx1, and no discernable ATP release from Panx2. Together, these results demonstrate that Panx1 opened by LPC shares similar ionic selectivity to previously reported modes of channel stimulation such as membrane depolarization or caspase cleavage and is also capable of ATP release. They also show that Panx2 opened by LPC shares similar selectivity for small inorganic ions but has a comparatively limited ATP permeability.

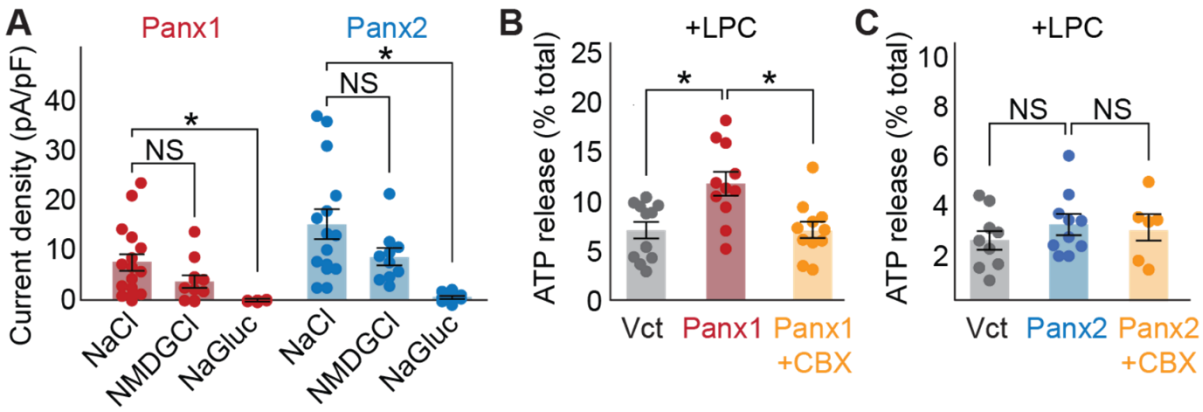

Figure 5. Permeation properties of Panx1 and Panx2 stimulated by LPC. **(A)** Peak whole-cell current densities obtained from Panx1 or Panx2 stimulated with LPC 16:0 (7uM) in symmetric solutions of the indicated salt. Asterisks represent statistical significance of a t-test where p-value < 0.05. **(B,C)** ATP release from cells treated with LPC 16:0 (30uM) with or without CBX (50uM). Data were normalized total ATP content of cells (see methods).

LPC opens Panx1 in proteoliposomes

While the current data demonstrate that LPC opens Panx1 and Panx2, it is still possible that LPC opens pannexin downstream of another protein such as the LPC G-protein receptor family[106]. To investigate if LPC acts directly, we assessed the ability of LPC to open liposome-reconstituted Panx1. As Panx1 uptake of the dye YOPRO is well-established, we incorporated DNA into the Panx1 proteoliposomes and measured their ability to uptake YOPRO when stimulated with LPC (Figure 6A). We found that LPC enhanced YOPRO uptake in a dose-dependent manner, but this effect did not occur in liposomes with no Panx1 incorporated (Figure 6A). Given the absence of all other cellular components in proteoliposomes, these data indicate that LPC acts directly on pannexins to induce channel opening.

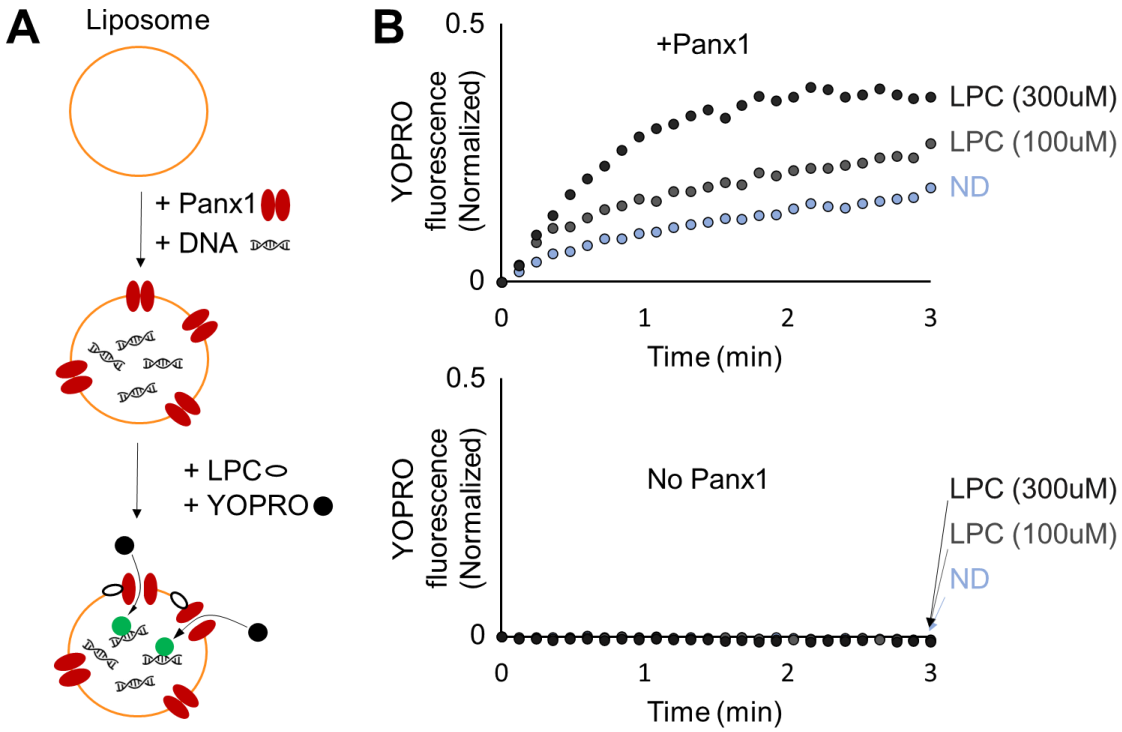

Figure 6. LPC opens Panx1 isolated in proteoliposomes. **(A)** Cartoon depicting incorporation of purified Panx1 and DNA into liposomes. Following incorporation, YOPRO and LPC were added to proteoliposomes. Upon opening of Panx1 due to LPC, YOPRO travels into the liposomes and binds to the DNA. DNA-bound YOPRO fluoresces green. **(B)** Representative traces of LPC applied to Panx1 proteoliposomes (top) or liposomes without Panx1 (bottom).

LPC may induce a reorientation of the Panx1 N-terminus from the cytoplasm into the pore

We sought to resolve the molecular mechanism for LPC channel gating by assessing any conformational changes induced by LPC with CryoEM. We previously determined the CryoEM structure of frPanx1 ΔLC, a modified frPanx1 construct with an internal loop deletion and C-terminal truncation, which greatly enhanced protein stability and monodisperisty[85]. We used this construct, adding the N-terminal insertion of GS (frPanx1(+GS) ΔLC) to enhance the channel channels response to LPC. The frPanx1(+GS) ΔLC was purified, reconstituted into MSP2N2 nanodiscs, and treated with LPC. The preliminary CryoEM results show the appearance of a density within the pore which most likely corresponds to the channels N-terminus (Figure 7A). This is because our previous structure did not display this density, and the LPC-treated structure does not appear to contain a density which corresponds to the cytoplasmically oriented N-terminus. Interestingly, a recent study of the Panx1 inhibition mechanism showed the same trend in reverse. Upon treatment with the Panx1 inhibitor probenecid, a pore-associated distal N-terminus relocated into the cytoplasm(Figure 7B)[87]. Thus, our results tentatively suggest that LPC opens Panx1 through a flip of the N-terminus from the cytoplasm into the pore.

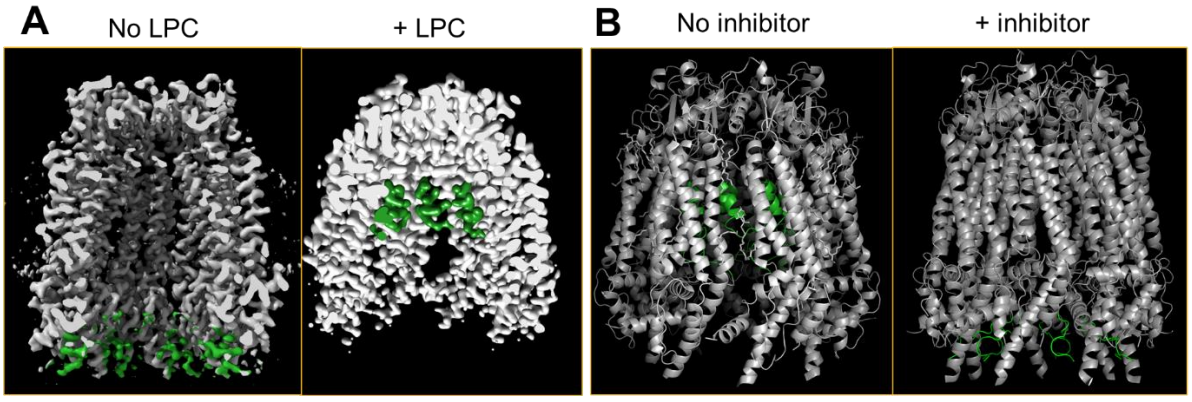

Figure 7. A density corresponding to the distal Panx1 N-terminus appears in the pore of LPC-treated Panx1. **(A)** (left) CryoEM map of our previously solved structure (PDB: 6VD7) of frPanx1 ΔLC displaying an N-terminus extending into the cytoplasm. The density corresponding to the distal N-terminus is colored in green. (right) Current preliminary map of frPanx1(+GS) ΔLC treated with LPC (100uM) which displays a prominent density within the pore not present in our previous map. **(B)** Structural models of a recent study of full-length hPanx1 where a pore-associated N-terminus (green) relocated to the cytoplasm upon treatment of the channel with the inhibitor probenecid.

The mVenus quench assay reveals a class of pannexin lysolipid agonists enriched in serum and synovia

There is a vast family of naturally occurring lysolipids, which vary in their lipid tail length, tail position, backbone, degree of saturation, and headgroup. We sought to determine the specificity of pannexin lysolipid agonism by testing different species of the lysolipid family with a higher throughput than patch clamp. To do so, we co-expressed pannexin with the halide sensing

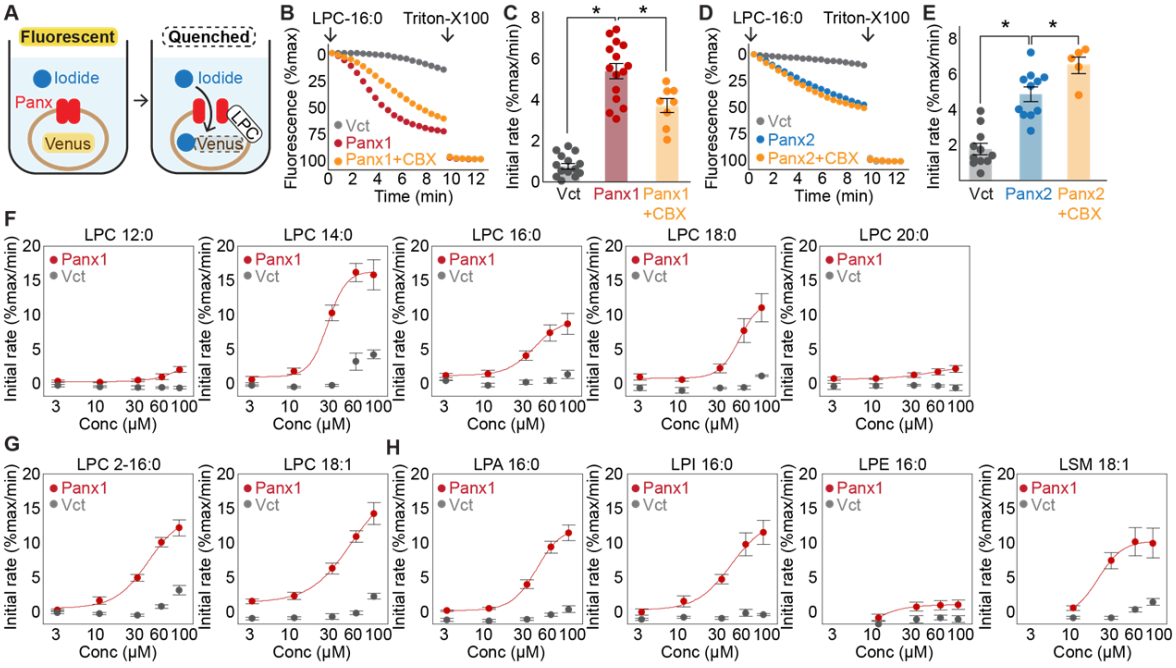

Figure 8. A cellular mVenus-quench assay reveals a family of lysolipid agonists. **(A)** Cartoon illustrating the principle of the mVenus quench assay. Buffer containing NaI is placed outside cells expressing mVenus and Panx. Panx opened by LPC will then allow iodide into the cell, quenching mVenus fluorescence. **(B)** Representative experimental trial of fluorescence quenching due to application of LPC-16:0 (30uM) and co-application of CBX (50uM) to GnTI- cells expressing mVenus alone (Vct) or mVenus and hPanx1 (Panx1.) **(C)** Quantification of initial rates obtained from all trials. Asterisks indicate statistical significance ($p < 0.05$) from an unpaired t-test. **(D)** Application of LPC-16:0 and co-application of CBX to 293 cells expressing mVenus or mVenus and hPanx2. (E) Quantification of initial rates from D. **(F-H)** Dose-response profile of the indicated lysolipid species for hPanx1. Lipid names describe the various saturated tail lengths of LPC (LPC 12:0 to LPC 20:0), the sn-2 version of LPC-16:0 (LPC 2-16:0), a monounsaturated version of LPC-18:0 (LPC-18:1), or other lysolipids with different headgroups (LPA-16:0, LPI-16:0, LPE-16:0) or backbones (LSM-d18:1).

mVenus in a 96-well plate format[107]. mVenus is a YFP which quenches upon iodide binding and can thus act as an optical readout for opening of the highly iodide-permeable pannexin channel (Figure 8A)[61,105]. We found that co-expression of Panx1 or Panx2 with mVenus produced a robust increase in LPC-induced quenching (Figure 8B-E). Further, CBX inhibited Panx1, but not Panx2-mediated quenching, indicating that the quenching is due to iodide permeation through LPC-opened pannexin channels.

Using this cellular mVenus quench assay, we assessed the ability of different lysolipid species to open Panx1 and Panx2. We found that LPC with saturated 14C to 18C-long tails worked to open pannexin with similar potency and efficacies (Figure 8F, Figure 8 continued I). This activity sharply decreased by shortening the tail length to 12C or increasing it 20C. Switching the position of the tail to the sn-2 position of the glycerol backbone or adding a kink in the tail through a single double bond, yielded comparable activity to their respective sn-1 and saturated tail counterparts (Figure 8G, Figure 8 continued J). We also tested lysolipids containing headgroups of the four major membrane glycerophospholipids, finding that all but lysoPE worked as pannexin agonists (Figure 8H, Figure 8 continued K). Finally, we tested the effect of a lysolipid with a sphingosine backbone, lysoSM. This lipid also worked comparably to its glycerophospholipid counterparts to open both Panx1 and Panx2.

In summary, we found that both the headgroup and tail composition determine lysolipid agonist efficacy for pannexin1 and pannexin2: lysolipids with intermediate tail lengths, and large neutral or acidic headgroups are agonists of pannexins in the range of 10-100uM. A subset of these lysolipid species, the LPCs, are present at similar concentrations in fluids of the body such as blood and synovia, and become enriched under inflammatory conditions such as rheumatoid arthritis or acute injury[108,109].

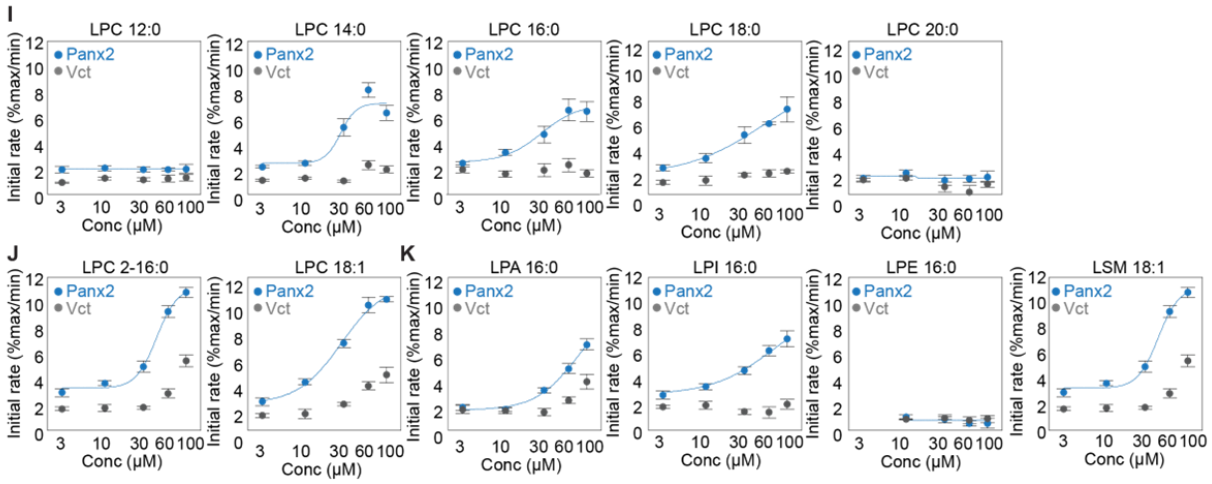

Figure 8 continued. (I-K) Dose-response profile of the indicated lysolipid species for hPanx2. Lipid name describes the various saturated tail lengths of LPC (LPC 12:0 to LPC 20:0), the sn-2version of LPC-16:0 (LPC 2-16:0), a monounsaturated version of LPC-18:0 (LPC-18:1), or other lysolipids with different headgroups (LPA-16:0, LPI-16:0, LPE-16:0) or backbones (LSM-d18:1).

The lysolipid-generating enzyme sPLA2 can open pannexin channels

One of the principal ways lysolipids are generated is through the phospholipase A2 (PLA2) family of enzymes. These enzymes catalyze the hydrolysis of membrane phospholipids, producing a lysophospholipid and a free fatty acid (Figure 9A). Of these, the secreted forms of PLA2 (sPLA2) hydrolyze phospholipids of the plasma membrane outer leaflet. We wondered if the production of lysophospholipids from outer leaflet phospholipids by sPLA2 enzymes could also open pannexin channels in the mVenus quench assay. Indeed, sPLA2 applied to cells induced pannexin-dependent quenching, which was inhibited by the application of CBX in the case of Pannexin1 (Figure 9B-E). PLA2 activity also produces free fatty acids such as arachidonic acid (AA), which also can be further metabolized to produce additional signaling molecules such as prostanoids and endocannabinoids. We therefore assessed the ability of pure AA, the prostanoids PGE2 and PGI2, and the endocannabinoid arachidonoylethanolamide (AEA) to induce pannexin-dependent quenching (Figure 9F). However, these metabolites failed to elicit increases in pannexin-dependent quenching. Together, these data show that sPLA2

enzymes can stimulate opening of pannexin channels, most likely by their production of lysolipids from the hydrolysis of membrane lipids.

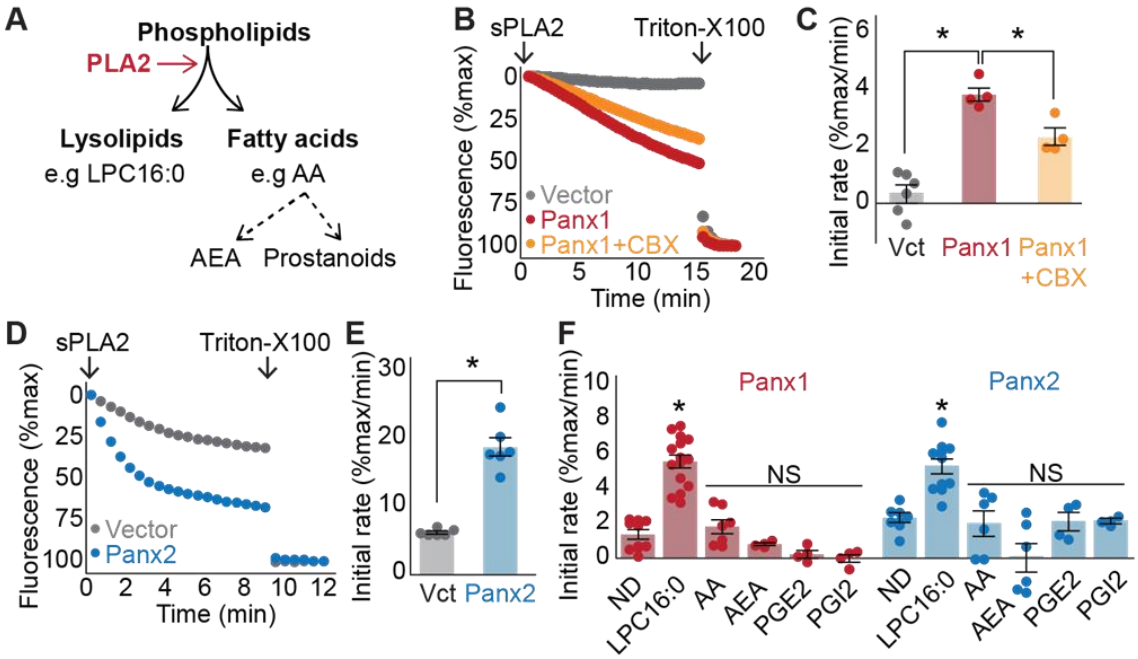

Figure 9. The lysolipid-producing enzyme PLA2 and the PLA2 activator mastoparan (MTP) induce pannexin channel activity. **(A)** Lysolipids and eicosanoids are produced from phospholipids by the enzyme PLA2. **(B, D)** Application of sPLA2 (0.14mg/mL) to hPanx1 and hPanx2. **(C, E)** Quantification of initial rates due to sPLA2 application. Asterisks indicate statistical significance ($p < 0.05$) from an unpaired t-test. **(F)** Application of major metabolic products of PLA2 activity and downstream eicosanoid synthesis to Panx1 and Panx2. A single factor one-way ANOVA followed by a one-way Dunnett's T-test was applied to assess statistical significance at $p < 0.05$.

The PLA2-activating peptide mastoparan stimulates Pannexin1 opening

PLA2 is activated by polycationic amphipathic peptides commonly found in the venoms of bees, snakes and other poisonous creatures. One such peptide is mastoparan, which increases purified sPLA2 hydrolysis rates by as much as 50-fold[110]. Additionally, mastoparan can induce cellular PLA2 activity in a variety of cell types[110–112], most likely due to its ability translocate across the plasma membrane and activate G-proteins by enhancing GDP/GTP exchange Figure

9 continued, G)[113,114]. Given that endogenous PLA2 activity has been demonstrated in HEK293 cells[115,116], we wondered if mastoparan application could stimulate PLA2-dependent opening of pannexins in our cellular mVenus quench assay. Application of mastoparan caused a robust, CBX-sensitive Pannexin1-dependent quenching (Figure 9 continued H, I).

Pannexin1 is known to open following the cleavage of its C-terminus by caspases during apoptosis and has been proposed to open following tyrosine phosphorylation of its cytoplasmic domains by SRC family kinases[15,58]. Since prolonged mastoparan application has been reported to induce apoptosis[117,118], and since G proteins are an effector of Src kinases,[119] Panx1 may open following mastoparan application by a caspase or Src-mediated mechanism. We applied mastoparan following preincubation of the SRC inhibitor PP2 or the pan-caspase inhibitor z-DEVD-fmk and found that neither inhibitor decreased mastoparan-induced pannexin1 opening (Figure 9 continued, I). Together, these data support the notion that mastoparan opens Panx1 through a PLA2-mediated mechanism.

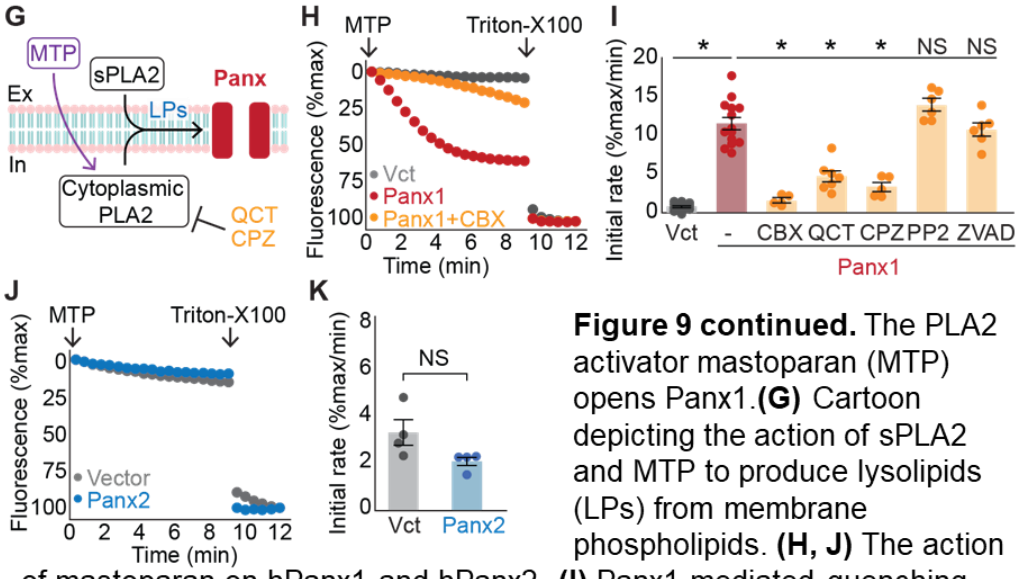

Figure 9 continued. The PLA2 activator mastoparan (MTP) opens Panx1.**(G)** Cartoon depicting the action of sPLA2 and MTP to produce lysolipids (LPs) from membrane phospholipids. **(H, J)** The action of mastoparan on hPanx1 and hPanx2. **(I)** Panx1-mediated quenching rate of MTP alone, co-applied with CBX or following pre-incubation with quercetin (QCT), chlorpromazine (CPZ), PP2, or ZVAD. **(K)** Initial quenching rates for hPanx2.

Discussion

Lysolipids directly and reversibly open pannexin through an N-terminal mediated mechanism

Triggers which directly and reversibly open pannexin channels have remained elusive for over 20 years. We established that lysolipids act as one such trigger for both Panx1 and Panx2, suggesting that this may be a general mechanism for controlling the pannexin gate. The biological implications of this are discussed below. We also found that LPC treatment of Panx1 may induce a reorientation of the N-terminus from the cytoplasmic side of the channel into the pore, while the N-terminus moves from the pore into the cytoplasm upon treatment with the inhibitor probenecid[87]. Given that a channel activator and inhibitor induce opposing conformational changes, this N-terminal reorientation may in fact be part of the general gating mechanism. A higher resolution structure of the LPC-treated Panx1 is necessary to confirm that the observed density is indeed the N-terminus. Alternatively, it could be LPC itself, though at present it is unclear how the presence of LPC within the pore would promote channel opening.

These findings stand in stark contrast to a recent proposal that the distal N-terminus is dispensable for Panx1 channel activation[55]. It is important to note that this interpretation relied on the small and weakly rectifying basal currents that are generated by the wild-type construct in the range of -80mV to +80mV. It is possible that the distal N-terminus is dispensable for these small Panx1-mediated leak currents but critical for the channel to adopt a large-pore conformation. This would explain why both groups reported that the consequence of deleting amino acids 2-20 is a ‘collapsed’ pore with a smaller extracellular constriction at W74.

Further investigation into the role of N-terminal pannexin gating is necessary to resolve these discrepancies. On this front, it is noteworthy that hydrophobic residues inserted into the distal N-terminus generate hyperactive Panx1 channels[63]. It is possible that these insertions generate novel contacts with the Panx1 intersubunit annular lipids, thus stabilizing the predicted open

state of the channel. Systematic mutagenesis studies to enhance or discourage the contacts made by the N-terminus with surrounding residues or with the intersubunit annular lipids in the predicted open conformation of the channel could be correlated with changes in ATP permeability, ionic selectivity or stimulus-dependent opening (eg voltage, lysolipids).

Panx1 as a central node for crosstalk between lysolipid and purinergic signaling

We find that LPC can induce ATP release through Panx1, which unites two previously unconnected signaling pathways important in the immune system and the vasculature. LPC and ATP exert a substantial set of overlapping effects through their abilities to induce secretion of pro-inflammatory cytokines, induce chemotaxis, and activate immune cells[20,23,106,120,121]. This overlap could in part be a consequence of LPC-stimulated ATP release from Panx1 channels. Indeed, a recent study demonstrated that LPC-induced cytokine secretion was dependent on CBX and probenecid-sensitive release of ATP from macrophages.[122] Confirming the identity of Panx1 as the ATP-releasing channel with genetic KO/KD is the necessary next step. Then, see if this finding generalizes to other Panx1-expressing cells of the immune system, endothelium or smooth muscle.

In the vasculature, oxidized LDL (oLDL), which contains large quantities of LPC, potentiates PE-induced vasoconstriction[123]. LPC and oLDL also potentiate RhoA-mediated vasoconstriction[124]. In both cases, the downstream mediators of the contractile response were not established. Given the abundant data on PE-induced vasoconstriction initiated by Panx1 ATP release[31,32,90], and the recent report that PE activates Panx1 through a RhoA-dependent mechanism[52], LPC-induced release of ATP via Panx1 may be the causal factor for oLDL enhancement of vasoconstriction. Testing the ability of Panx1 blockers or Panx1 KO of VSMC to prevent vasoconstriction by oLDL/LPC would provide valuable information on this front.

Atheroprotective roles of Panx1 may be mediated by LPC:

Macrophage uptake of LDL particles is greatly enhanced following oxidation-dependent conversion of LDL-bound PC to LPC by endothelial cells[125], where as much as 40% of the LDL-PC content is hydrolyzed to LPC. This means that the processing of LDL-bound lipids by endothelial cells itself generates an abundant LPC signal which may stimulate Panx1 channels in the surrounding tissues. This would induce recruitment of macrophages to the local plaque, as has been reported for leukocyte recruitment via Panx1-released ATP by endothelial cells[23]. Once the macrophage has entered the lesion, LPC and ATP signals could also then help the macrophage find the modified LDL particles that it has the ability to engulf, as it is known that LPC itself is a chemotactic signal for macrophages and monocytic cells[126]. In this way LPC may amplify its own promigratory effects by increasing Panx1-mediated ATP release from endothelial cells. Consistent with this notion, endothelial cell KO of Panx-1 causes increased atherosclerotic lesions in arteries of atherogenic mice[25]. Alternatively, excessive LPC accumulation (perhaps due to hypercholesterolemia or large quantities of consumed oxidized lipids) may cause gratuitous macrophage invasion into the sub-endothelial space and promote hardening of plaque.

Possible role of lysolipid-Panx1 signaling in arthritic and damaged joints

We found that a subset of LPC species (C14-C18) open pannexins, and these closely match the enriched LPC species found in fluids of the body such as plasma and synovia[104,108]. In damaged joints, synovial concentrations of LPC can increase as much as ten-fold[108], whereas absolute concentrations in rheumatic and injured joints have been measured in excess of 100uM[127,128]. This means that the range of synovial LPC concentrations between healthy and inflamed joints (~10-100uM) spans the effective dose-response range of pannexins. Further, release of ATP via Panx1 was recently reported in synovial fibroblasts[129], and it is known that ATP efflux from cells comprising the synovial joint is a key step in RA pathogenesis[130]. Panx1 ATP release is also an important initiating step in tissue repair[131]. Together, these data suggest a functional role

of lysolipid-triggered ATP release via Panx1 during tissue repair, or as a pathological factor in conditions such as RA.

PLA2-Pannexin signaling axes represent a new avenue of inquiry into pannexin regulation

We also demonstrated that PLA2 enzymes can trigger pannexin channel opening, most likely by their production of lysolipids from the cell membrane. Further, the PLA2-activating peptide mastoparan opens Panx1, possibly by stimulating endogenous PLA activity in HEK293. These findings reveal a biochemical pathway that generates the first known pannexin agonist. They also suggest that downstream activation of lysolipid producing enzymes may account for many documented, but largely uncharacterized receptor-mediated modes of Panx1 channel stimulation[15]. To this end, it is interesting to note that stimulation of P2X7 receptors induces PLA2 activity in a variety of cell types[132]. In some instances there is also channel activity pharmacologically consistent with Panx1 channels downstream of P2X7 stimulation[133–135]. Thrombin stimulates robust PLA2 activity in platelets and myocytes[136,137]. Thrombin stimulation of platelets and endothelial cells generates CBX and probenecid-sensitive ATP release[138–140]. TNF-α also stimulates PLA2 activity in a variety of cell types where pannexins function has been demonstrated[141–144]. Hypotonic swelling also induces PLA2 activity[115,145,146]. In summary, many of the receptor-mediated and cell-swelling pathways that lead to Panx1 channel opening also stimulate PLA2-dependent production of lysolipids. It would therefore be informative to assess the involvement of PLA2 in these pathways.

The role of PLA2 in various inflammatory disorders: Pannexin as a missing link

The superfamily of PLA2 enzymes (cPLA2, iPLA2, sPLA2) contribute to many aspects of inflammation and inflammation-associated disorders such as heart disease, arthritis, diabetes, autoimmune disease and recently Sars-CoV2[147]. This is most commonly attributed to the liberation of ω-6 fatty acids such as AA by PLA2 lipid hydrolysis, which is a precursor for many

pro-inflammatory eicosanoids. This has led to a whirlwind of drug development against various PLA2 subtypes, but so far none have passed phase III clinical trials. One of the speculated reasons for this is that PLA2 enzymes also generate the precursors for inflammation-resolving eicosanoids such as ω-3 fatty acids. This means that inhibiting a given PLA2 subtype may have a net neutral effect on the component of inflammation mediated by PLA2-derived fatty acids. On the other hand, the effect of the lysophospholipids generated by PLA2 activity are comparatively less characterized. Given the well documented inflammation-promoting role of pannexin, lysophospholipid activation of Panx1 may be a missing link between PLA2 and diseases of inflammation. This would also provide an attractive clinical target, given that Panx1 inhibition would not in principle interfere with eicosanoid synthesis.

Roles of Panx2 LPC signaling and the possibility of Panx3 lysolipid activation

The potential roles of Panx1 lysolipid signaling may generalize to the other two pannexin family members, as compensatory upregulation of Panx3 in response to Panx1 KO/KD has been clearly demonstrated, and functional redundancy between Panx1 and Panx2 occurs in ischemic stroke[49]. Outside of redundant roles, the physiological significance of LPC opening Panx2 is presently unclear, as the roles of Panx2 remain mostly undefined. A few studies have established a role of Panx1 and Panx2 in enhancing insulin secretion from beta cells[93,94]. As LPC levels also can enhance insulin sensitivity and can predict diabetic outcomes[148], there may be crosstalk between insulin sensitivity and phospholipid metabolism that is mediated by Panx1 and Panx2. Further work could investigate this possibility by first seeing if LPC can open the pannexins expressed on beta cells. There is also evidence for Panx2 functioning as an ER channel[14,149,150]. This suggests a role for the intracellular cPLA2 enzymes in opening ER-associated Panx2, given that activated cPLA2 translocates to and subsequently hydrolyzes lipids of the ER membrane.

We do not yet know whether Panx3 is also a lysolipid-gated channel, given that, like previous groups, we were unable to establish that Panx3 forms functional channels at the plasma membrane in our heterologous expression systems. Since both Panx1 and Panx2 are lysolipid gated channels and Panx1-3 are highly similar, it seems more likely that Panx3 is also opened by lysolipids. Some groups have shown clear Panx3-mediated ATP release and dye uptake from myocytes and skin cells indicating that Panx3 does function as a plasma membrane channel under the right conditions[11]. It is tempting to speculate that, like Panx1, there are specific post-translational modifications of Panx3 which convert the silent channel into a primed form capable of stimulus-dependent opening. To this end, it would be interesting to see if any specific Panx3 PTMs are highly enriched in myocyte/skin cell Panx3, as compared to the heterologously expressed version in HEK293. It would also be interesting to see if Panx3-mediated currents or small molecule flux could be recorded from lysolipid-stimulated myocytes/skin cells. On the other hand, like Panx2, Panx3 functions as an ER channel[11]. It may also then be activated by ER-derived lysolipids via cPLA2 activity.

Chapter 2: A C-terminal domain is necessary for activation of Panx1

Introduction

Pannexin1 (Panx1) is a broadly expressed ion channel that can release various small molecules such as ATP. It has important signaling roles in the immune system, cardiovascular system, and nervous system. Dysregulated Panx1 activity is associated with inflammation-related pathology in these systems such as asthma, aortic aneurysm, atherosclerosis, and ischemic neuron death. The ability to regulate Panx1 activity pharmacologically therefore presents a novel clinical lever to pull for improvement of disease outcomes. Currently, there are no known specific, potent, and efficacious Panx1 inhibitors or activators, which represents the primary barrier to manipulate Panx1 activity in clinical and basic research. The ability to generate these channel modulators would be greatly facilitated by an understanding of the channel's activation mechanism.

In the prevailing mechanism of Panx1 channel activation, a pore-associated distal C-terminus (amino acids 380-426) blocks the cytoplasmic side of the conduction pathway. Upon removal of this region by caspase3/7 cleavage, or relocation due to conformational change, the pore pathway is then cleared, resulting in ion conduction. This is supported by the findings from many labs that any Panx1 construct which terminates at or near the caspase cleavage site (D379 for hPanx1) yields constitutively open Panx1 channels[51,53–56]. Further, caspase cleavage is sufficient to induce Panx1-dependent dye uptake and ionic currents when highly purified Panx1 is incorporated into liposomes or planar bilayers[57,58]. These data conclusively show that removal of the distal C-terminus is sufficient to open Panx1.

While the C-terminal pore block model is supported by these data, there are several recent findings which indicate it is incomplete. Our lab obtained a high-resolution structure of a frPanx1 channel (frPanx1 ΔLC)[85]. This construct is C-terminally truncated 24 residues upstream (355) of the caspase cleavage site (379), which increases protein yield, stability and homogeneity. Yet,

this aggressive truncation yields a channel even less active than full-length Panx1. frPanx1 ΔLC is shut except when extreme and sustained positive voltages are applied to the cells but, like the full-length form, can be hyperactivated by modifying the N-terminus. The discoverers of cleavage-based Panx1 activation also recently reported that the same truncation resulted in silent channels which are still activated downstream of adrenergic receptor stimulation[54]. The simple 'pore-plug' mechanism cannot explain these findings, as they show that the channel can shut and open independently of the distal C-terminus. They also imply that C-terminal activation of Panx1 requires an additional undefined domain upstream of the caspase cleavage site.

I searched for this domain using sequential genetic deletions of the Panx1 C-terminus and assessing their activity by whole-cell patch clamp. I discovered two leucine residues critical for channel activation, contained within a predicted alpha helix just upstream of the caspase cleavage site. I also found that an adjacent region is necessary for activation by divalent cations, a novel form of channel stimulation we recently discovered. Analysis of the available Panx1 structures revealed that the helix necessary for cleavage activation localizes to a site which can alternatively be occupied by the distal N-terminus. These findings provide a tentative first basis the general Panx1 activation mechanism, which is briefly discussed.

Methods:

Molecular Cloning and Obtained Plasmids

All constructs were subcloned into either pIM2 or pIE2 vectors using 5' end and 3' end XhoI cloning sites introduced by PCR. This results in a Gly-Ser insertion after the first methionine and an Ala-Ser-Ser insertion before the stop codon. In Panx1-containing constructs, the Gly-Ser and Ala-Ser-Ser insertions were removed by site-directed mutagenesis. All point mutants were made by site-directed mutagenesis.

Cell Culture and Transfection

Human embryonic kidney (HEK293) cells were cultured in growth medium supplemented with 10%FBS and incubated at 5% CO_2 and 37˚C. For electrophysiological studies, HEK cells were plated onto 12mm glass coverslips, then ~24 hours later co-transfected with either a pIE2 or pIM2 plasmid encoding the indicated constructs. The transfection protocol was as follows: to 100uL transfection media (Gibco Optimem(1X), Glutamax), 600-800ng total DNA and 3uL transfection reagent (Promega Fugene6) was added, mixed, then incubated for 10-15 minutes at RT. Electrophysiological recordings were performed 24-72 hours after transfection.

Electrophysiology

All experiments were performed with an Axopatch 200B patch clamp amplifier, Digidata 1440A digitizer, an Axon CV-203B0 headstage and recorded using pClamp10 software. A fluorescence lamp was used to visualize successfully transfected cells. Recordings were sampled at 10kHz and filtered to 2kHz prior to analysis. Glass micropipettes (1.5OD, 0.86ID, 75L, Harvard Apparatus) were pulled (P-1000, Sutter Instruments) and fire polished (MF-200 Microforge), yielding 1.5-4MO pipettes for inside-out and whole-cell patches. For all recordings, the bath solution contained (in mM) 147 NaCl, 2KCl, 2 $CaCl_2$, 1 $MgCl_2$, 10 HEPES, and 13 Glucose adjusted to pH 7.3 using NaOH. Whole-cell patch pipette solution contained (in mM) 147 NaCl, 10 HEPES, and 10 EGTA adjusted to pH 7.0 using NaOH. For inside-out recordings, pipettes contained the bath solution. Inside-out patch perfusion buffer contained (in mM) 155 NaCl, 10 HEPES and 0.1 EGTA adjusted to pH 7.0 using NaOH unless otherwise indicated.

Inside-Out Patch Protocol and TEV Protocol

Inside-out patches were obtained by brief air exposure of patches pulled from Panx1-expressing cells. Where voltage steps are shown, voltage steps from -110mV to +110mV were used to indicate the presence of Panx1 channels in the patch.

To measure the effect of TEV on hPanx1-mediated currents, a voltage ramp protocol (V_A= +130mV to -80mV) was applied every 6 seconds. After 10 minutes, TEV protease (100ug/mL) was perfused onto the inside-out patch. Every 5 minutes, 100uM CBX was applied for 2 voltage ramps.

TEV protease (TEVp) purification protocol

TEVp was subcloned into the pNNG-BC10 vector to generate an N-terminal 8His tag, then transformed into BL21 competent cells. It was then purified by nickel affinity chromatography essentially as described for srcCD (see chapter 3, methods). Instead of SEC, buffer was exchanged by serially concentrating and diluting with TBS + 10% glycerol. Protein was flash-frozen in liquid N_2 and stored at -80°C.

Purification of Panx1 371 AA ΔL

Panx1 372 AA ΔL was purified from High five insect cells as described in chapter 3 methods for frPanx1 ΔLC.

Results

Sequential truncations of hPanx1 reveal the activating and auto-inhibitory regions

To gain a more accurate understanding of the Panx1 activation mechanism, I sought to find the C-terminal activating domain (CAD) missing in our truncated frPanx1 ΔLC construct. I also wanted to identify the C-terminal inhibitory domain (CID). To do this, I assessed the channel activity of truncated hPanx1 constructs with whole-cell patch clamp. From the distal C-terminus, deletions surpassing amino acid 410 yielded successively more channel activity (Figure 1A). By amino acid 391 the truncated channel was as active as the truncation mimicking caspase cleavage (379). This activity persisted until 370, upon which a single additional deletion (369) and all subsequent deletions resulted in essentially inactive channels, characteristic of the full-length Panx1.

To find the residues mediating the effect of the CAD, I made alanine substitutions in the residues upstream and downstream of 369 in the background of 1-371 to see if CAD activity could be abolished. Individually, L370A and L367A both reduced channel activity (Figure 1B), and the double alanine substitution L370A/L367A completely abolished channel activity. This channel is still functional, as it can be opened by other means (see chapter on divalent activation, Figure 6B). To further confirm that this double substitution prevents cleavage-mediated activation of hPanx1, the L370A/L367A substitutions were made in full-length hPanx1 with the caspase cleavage site switched for a TEV cleavage site (hPanx1T and hPanx1T AA). Upon co-expression of hPanx1T with TEVp, whole-cell currents developed, indicating cleavage-mediated activation (Figure 1C). However, no such currents develop when hPanx1T AA is used instead. The same trend was seen when TEVp protein was perfused to the cytoplasmic side of an inside-out patch pulled from cells expressing either hPanx1T or hPanx1T AA (Figure 1D). These data strongly suggest that L370 and L367 play a critical role in the cleavage-mediated activity of Panx1.

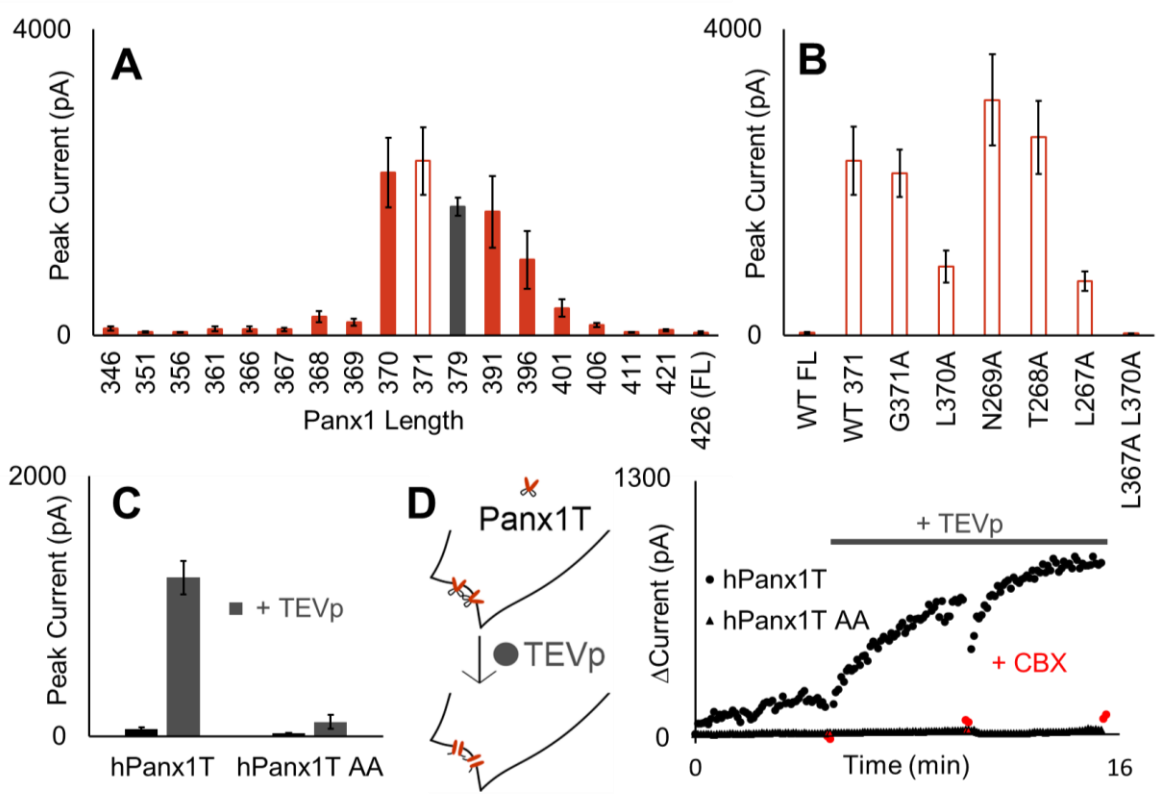

Figure 1. Cleavage-mediated activation of Panx1 requires a C-terminal activating domain. **(A)** Peak whole-cell currents at +110mV obtained from HEK293 cells expressing truncated hPanx1 constructs which terminate at the indicated residue. FL denotes the full-length channel, and 379 terminates at the caspase cleavage site. **(B)** Whole-cell currents obtained from alanine substitutions made on the truncation construct 371. **(C)** Whole-cell currents of hPanx1T or hPanx1T AA with or without co-expression of TEVp. **(D)** Left, Perfusion of TEVp onto hPanx1T channels in an inside-out patch cleaves the C-terminus, leading to open channels. Right, the change in currents from hPanx1T or hPanx1T AA inside-out patches before and after TEVp (0.1mg/mL) perfusion (grey bar). The inhibitor CBX (50uM) was used to confirm the currents were Panx1-mediated.

The CID region is comparatively diffuse

In contrast to the few individual amino acids controlling the effect of the CAD, the CID is distributed throughout ~20 amino acids (Figure 1A), which are disordered and not resolved at all in any current structure. This suggests that a series of low affinity, high avidity contacts made throughout this region keep the channel inactivated. Consistent with this notion, an earlier study found that randomly scrambling the order of the distal C-terminal amino acids produced variably

active channels, with some scrambled constructs displaying activity comparable to the caspase-cleaved form and others as inactive as full-length Panx1[151].

Nevertheless, if the CID is a discrete but diffuse domain, then deletions of the CID should activate the channel. I performed internal deletions of 5 and 10 amino acids in the 20 amino acid stretch (392-410) that successively activated Panx1 upon truncation. I found that one internal deletion (392-396) partially relieved channel block (Figure 2). This agrees with the fact that truncations up to amino acids 392-401 caused the largest increases in channel activity. How this region acts to inhibit the channel remains an open question, but it may interact with the CAD to prevent it from binding to an activation site. Then, upon cleavage or rearrangement of the distal C-terminus, the CAD is liberated. Alternatively, the distal C-terminus containing the CID may have an interaction partner which 'pins' the C-terminus so as to keep the CAD away from its active binding site.

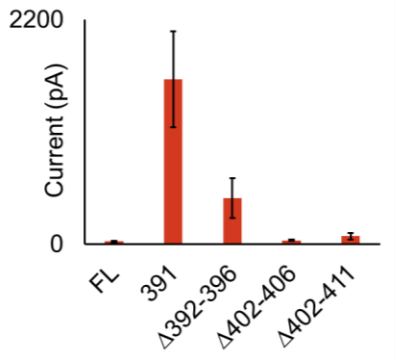

Figure 2. Internal deletions of the CID region partially activate Panx1. Peak whole-cell currents from hPanx1 constructs with the indicated internal deletions. Currents are compared to the truncation construct 391, which has the entire autoinhibitory region and subsequent residues deleted.

Panx1 activation by divalent cations offers an alternative stimulus to study CAD relevance

The identification of the CAD and CID provide a deeper understanding of the mechanism for activation of Panx1 following C-terminal cleavage. Yet, it is unknown if this domain is important for channel regulation in general. In parallel to studies of the CAD, I found that divalent cations are a novel gating stimulus for Panx1. Given the lack of known Panx1 activators, this afforded an opportunity to assess the relevance of the CAD to forms of channel activation outside of C-

terminal caspase cleavage. I describe the principal findings of divalent activation here, and then their relevance to the CAD mechanism.

Panx1 in excised patches is opened by cytoplasmic application of divalent cations at depolarized membrane potentials

I found that select divalent cations (Mn^{2+}, Co^{2+} and Mg^{2+}, but not Ca^{2+} or Zn^{2+}) can open Panx1 when applied to the cytoplasmic face of inside-out patches held at +50mV (Figure 3). A large, irreversible current develops over the course of a minute or two, which can be reversibly blocked by the Panx1 inhibitor CBX. This current does not develop at all in mock-transfected cells. This discovery suggested that Panx1 may have a biological function as a channel gated by rises in cytoplasmic free [Mg^{2+}], which can reach the low mM concentrations required to stimulate this activity. However, additional characterizations suggest that Mg^{2+} is unlikely to induce Panx1 currents in general.

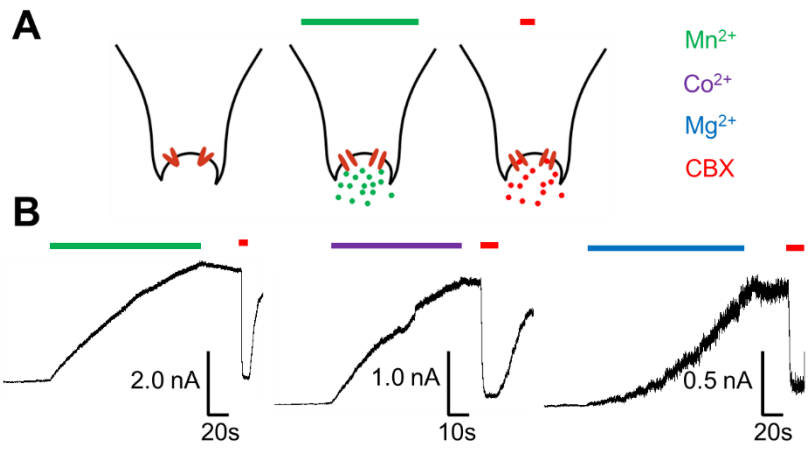

Figure 3. Cytoplasmic application of divalent cations open Panx1 channels. **(A)** Cartoon showing application of divalents to Panx1 inside-out patches, washout, and subsequent CBX application. **(B)** Exemplar currents generates from divalent application to inside-out patches pulled from HEK293 cells expressing Panx1.

While depolarized Panx1 outside-out patches also develop modest currents when Mn^{2+} is included in the pipette tip (Figure 4A), whole-cell patches do not (Figure 4B). Additionally, simultaneous depolarization is required for Mn2+ to open Panx1 (Figure 5). This indicates that divalents are acting through Panx1 itself, as there are no known voltage-dependent enzymes

which are also activated by divalent cations. However, the required voltage to realize the effect of divalents is also unphysiological.

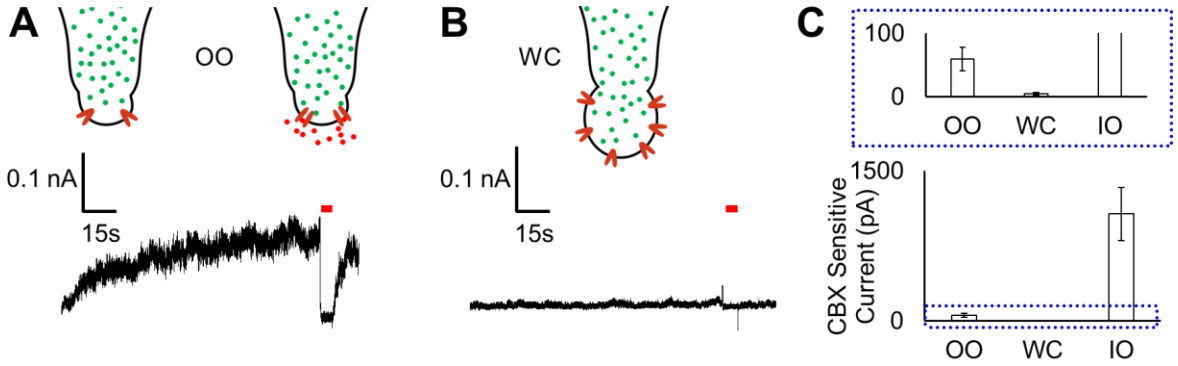

Figure 4. Divalent-stimulated currents only work in excised patches. **(A)** Outside-out (OO) patch with 3mM Mn2+ included in the pipette tip. Patch was stepped to +50mV for the duration of the recording. Red bars indicate CBX (50uM) application. **(B)** Whole-cell patch (WC) challenged with same protocol. **(C)** Average CBX-sensitive currents after 2 minute divalent stimulation.

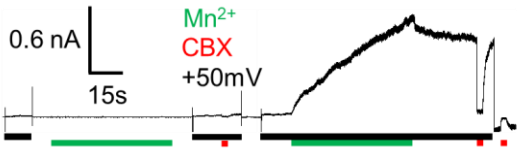

Figure 5. Divalent stimulation requires simultaneous membrane depolarization. Exemplar recording of a hPanx1 inside-out patch exposed to 2mM Mn2+ at resting membrane potential (-70mV) or +50mV (black bars).

The site of divalent activation lies in the C-terminus near the CAD region

While the biological relevance is presently unclear, divalent stimulation of Panx1 afforded a new opportunity to dissect the channels activation mechanism using structural studies. To this end, I first sought to find the regions of the channel necessary for divalent action. This would allow me to engineer a construct optimized for stability, yield and homogeneity that still responded to divalents. The C-terminal deletion used in our previous structural studies of frPanx1 (hPanx1 355) did not respond to divalents (Figure 6). As with frPanx1, hPanx1 355 can be stimulated to open by voltage when +GS is added, indicating that it forms functional channels (Figure 6). This suggested that the CAD may be involved, so I tested hPanx1 371 AA, the construct which contains the CAD but is rendered inactive by a double leucine-alanine substitution. This construct retained the ability to generate robust responses to divalents (Figure 6). I therefore

tested additional truncations and found that hPanx1 361 also responded robustly. I tried, but ultimately failed to find specific residues in between 356 and 361 that mediated the divalent response. Nevertheless, these findings indicate that divalents site of action is distinct but may overlap with the key residues for cleavage-mediated activation. Based on this, we opted to use hPanx1 371 AA for structural studies. This is because the large C-terminal truncation and inactivating substitutions should improve protein behavior (stability, homogeneity, yield), but it still contains the residues which roughly comprise the domain for both divalent and cleavage-mediated activation.

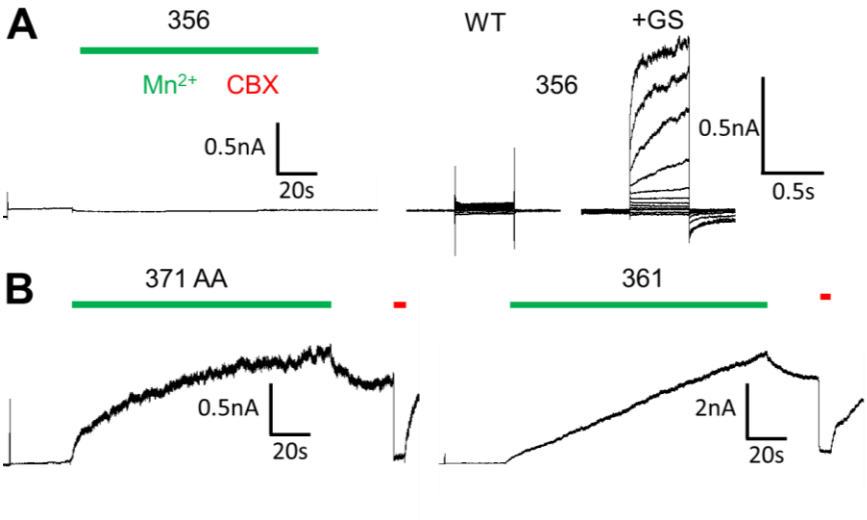

Figure 6. Divalent stimulation requires an undefined portion of the CAD-adjacent C-terminus. **(A)** Mn^{2+} treatment of hPanx1 truncated to residue 356 (356) does not induce inside-out patch currents. Whole-cell currents from WT 356 and 356 with the N-terminal GS insertion. **(B)** Mn2+ application to CAD inactivated construct 371 AA and truncation construct 361.

CryoEM of Mn^{2+}-treated hPanx1 yields inconclusive results

We sought to visualize the effect of divalents by treating hPanx1 371 AA with Mn^{2+} and assessing its structure by CryoEM. To do so, I first performed one additional modification to the channel: An internal loop deletion previously found to enhance protein monodispersity and stability[85]. I confirmed that the channel still opened following divalent application (Fig 7), then expressed and purified it from insect cells (Fig 7). The protein purified with sufficient yield and stability for MSP nanodisc reconstitution. I performed reconstitution into MSP2N2 nanodiscs and isolated the reconstituted Panx1 by SEC (Fig 7). We then analyzed the structure of this sample

by CryoEM following treatment with 10mM Mn^{2+}. Unfortunately, 3D reconstruction yielded a map with poor resolution (~>5Å global resolution), which did not enable us to identify any potential differences in the conformation with respect to the rest of the deposited Panx1 structures. We therefore did not further pursue a high-resolution structure using this construct and purification strategy.

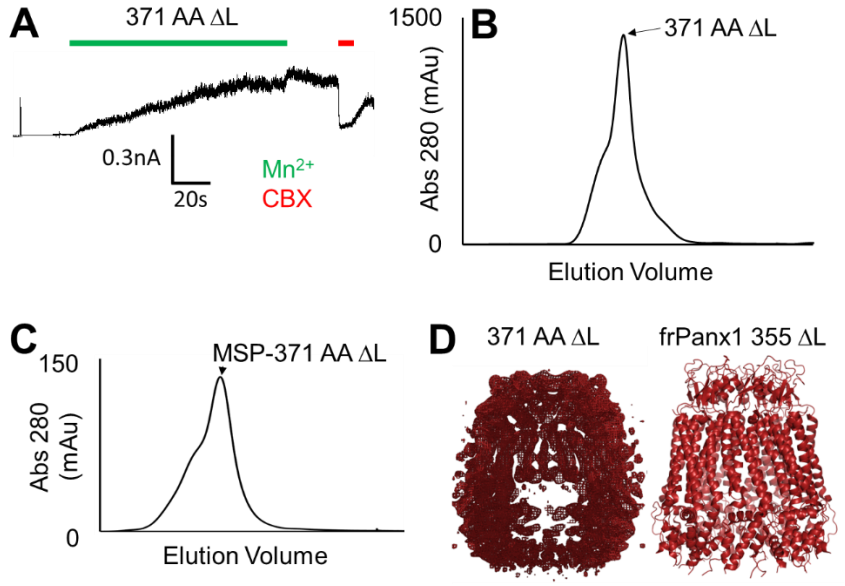

Figure 7. Purification and CryoEM analysis of optimized expression construct 371 AA ΔL **(A)** Mn^{2+} treatment of hPanx1 371 AA with an additional intracellular loop deleted (ΔL). **(B)** SEC elution profile of the purified construct. **(C)** Elution profile following reconstitution into MSP2N2 nanodiscs built with 3:1:1 POPE: POPG: POPC lipids. **(D)** Preliminary map versus our previously obtained structure.

Discussion

To determine the activation mechanism of Panx1, I sought to find the regions of the protein necessary for cleavage-mediated activation (CAD) and inhibition (CID) of Panx1. I located the CAD to a helix, where two leucine residues (L367 and L370) play a critical role in mediating cleavage-induced activation. I also found that the CID is comprised of a disordered region that likely makes many weaker interactions distributed throughout a 20 amino acid stretch (392-410).

Clues for the Panx1 activation mechanism in the currently available structures: A common binding pocket for both the CAD and the N-terminus

Though CryoEM efforts to resolve the effect of divalents and the CAD are ongoing, a recently deposited structure of hPanx1 resolved the backbone of the C-terminus up to amino acid 373

(Figure 8A)[55]. The CAD and divalent-sensitive region localize to a loop turn (356-361) and an alpha helix (362-372). This helix sits in a cytoplasmic pocket formed by an upstream C-terminal helix and part of an intracellular loop helix (Figure 8A, magenta helix). Yet, in our structure of the inactive frPanx1 ΔLC, this CAD contact site is instead occupied by the distal N-terminus.

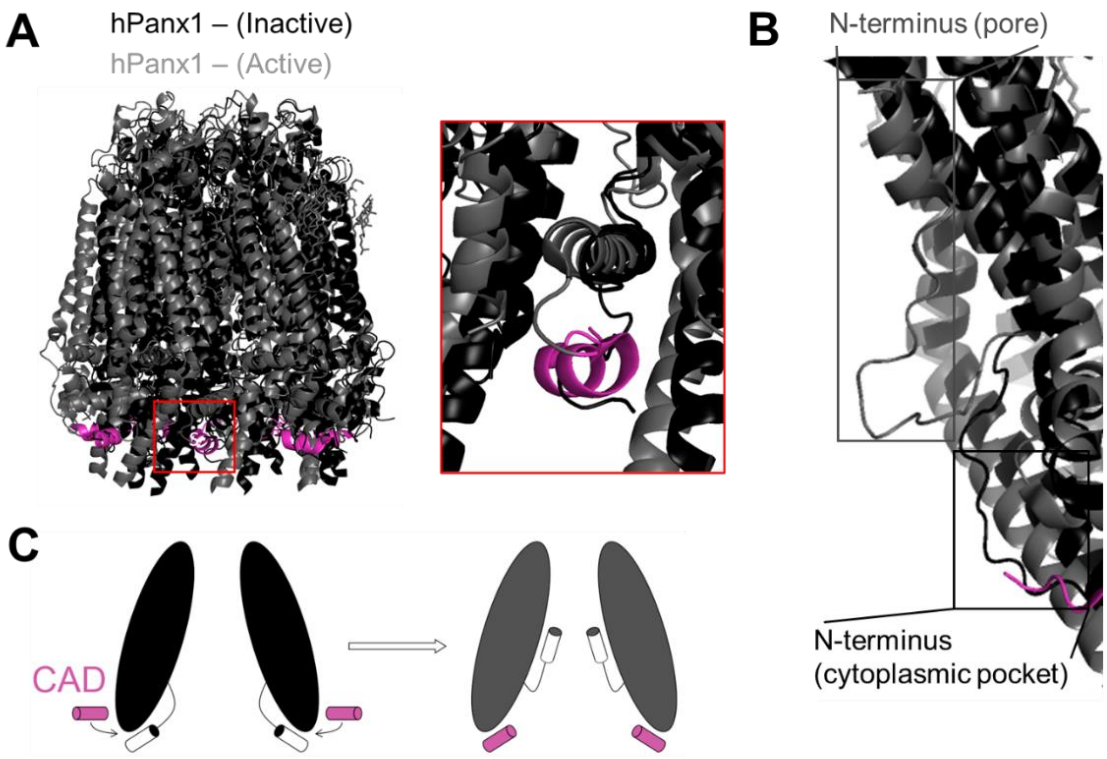

Figure 8. A mechanism for Panx1 channel activation by CAD-mediated liberation of the N-terminus. **(A)** Superimposed structures of an active (C-terminally cleaved, PDB:) and an inactive (probenecid-treated, PDB:) full-length hPanx1 channel. Red inset displays the overlapping site of the CAD helix (magenta) in the active channel form and the distal N-terminus (black disordered loop) of the inactive form. **(B) Single subunit side view** of superimposed active and inactive Panx1. The distal N-terminus within the pore of the active channel (grey) forms a helix, while in the inactive form, it extends into the cytoplasmic pocket as a disordered loop (black). **(C)** Cartoon of the possible activation mechanism of Panx1, which involves a reorientation of the N-terminus from the cytoplasmic into the channel pore, catalyzed by competitive binding of the CAD for the cytoplasmic pocket.

Another recent structure of hPanx1 treated with the inhibitor probenecid also found the N-terminus in this cytoplasmic pocket (Figure 8A, black disordered loop)[87]. In this work, they

proposed an unconventional gating mechanism, where membrane lipids move in and out of the channel pore between adjacent Panx1 subunits to respectively occlude and clear the permeation pathway. This was proposed because the pore became occluded with lipid-like densities only after they treated their sample with the widely used Panx1 inhibitor probenecid. This was accompanied by a displacement of the distal N-terminus (1-20) from within the pore into the cytoplasm. Since the pore-associated N-terminus binds within a cavernous hydrophobic interface between adjacent Panx1 TM helix bundles, they concluded that the relocation of the distal N-terminus into the cytoplasm allowed membrane lipids to migrate into the pore.

In the structure with the CAD backbone resolved, the N-terminus is in the pore-associated conformation (Figure 8B, grey). This suggests that the CAD may displace the cytoplasmically-associated N-terminus, which then relocates to the pore and opens the channel (Figure 8C), perhaps by displacing intrapore lipids. To see if this mechanism is accurate, it would be insightful to use a stimulus such as divalent cations or lysolipids on a CAD-intact Panx1 construct which displays an N-terminus extended into the cytoplasm (closed). Then, if the CAD moves to that position and the N-terminus reorients into the pore, this will provide compelling support for this activation mechanism. The fact that lysolipids may induce the reorientation of the N-terminus in the absence of the CAD (see Chapter 1, frPanx1 355 ΔL (+GS) was used) suggests that the activating effect of the CAD can be over-ridden. However, it is important to note that the activating N-terminal mutation +GS was used in this construct, so the wild-type channel may nevertheless require the CAD for its general regulation mechanism.

Chapter 3 : Panx1 is shut by a potential novel phosphoregulatory site Y10

Panx1 is an ion channel expressed throughout the body which mediates the cellular flux of diverse signaling molecules such as purines, glycolytic metabolites, amino acids, and endocannabinoids[10,19,58,152]. As a conduit for these important signaling molecules, Panx1 contributes to diverse aspects of physiology such as the constriction of peripheral arteries[31,32,90], leukocyte recruitment to areas of inflammation[23], neuromodulation[152], neuropathic pain[50], and the death of oxygen-deprived neurons[49]. Yet, while much is known about the roles that Panx1 plays in physiology, the molecular mechanisms of Panx1 channel regulation are largely unelucidated.

In all the aspects of (patho)physiology listed above, Src kinase-dependent phosphorylation of Panx1 has been found to be necessary for or correlate with increased Panx1 channel activity. This has led to the notion that Panx1 may be a phosphorylation-gated channel. For example, Src kinase-dependent phosphorylation of Panx1 at C-terminal Y309 coincides with a large, Src-dependent inward current in neurons blocked by the Panx1 inhibitor 10Panx1[153]. Src kinase also phosphorylates Panx1 at the intracellular loop residue Y199, and the Src-dependent release of ATP via Panx1 was ablated from channels harboring a Y199A mutation[23,34]. However, basal phosphorylation at Y199 occurring on silent Panx1 channels suggests that Y199 phosphorylation itself may not stimulate Panx1 ATP release[35]. It does, however, appear to be required for the Src-dependent release of ATP. Further, Src-dependent channel activity merely coincides with Panx1 Y309 phosphorylation, leaving open the possibility that Src kinase has additional or separate effects that lead to Panx1 opening. Thus, the relationship between the phosphorylation status of Panx1 and its Src-dependent channel activity is still unclear.

We sought to clarify this relationship by studying the effect of Src kinase on Panx1 channel function using patch clamp electrophysiology in a minimal cellular heterologous expression system, HEK293. We also used point mutations which mimic phosphorylation at Y199 and Y309

to isolate the potential impacts of phosphorylation in the absence of other Src-mediated signaling effects. We then expanded our investigation to include all 9 cytoplasmic tyrosine residues. Finally, we attempted to directly manipulate Panx1 channel activity in real time by applying Src kinase and a tyrosine phosphatase to Panx1 isolated in membrane patches.

Methods:

Molecular Cloning and Obtained Plasmids

All Panx1 constructs were subcloned into the BamHI/XhoI site of a pIE2 vector[78], which indicates successful transfection by concomitant EGFP fluorescence. The N-terminal Gly-Ser insertion into Panx1 which results from this cloning strategy was removed using the Agilent (Santa Clara, CA) Quikchange II PCR kit according to manufacturer's instructions. The full-length *gallus gallus* C-Src and V-Src genes were a kind gift from Richard Cerione (Cornell University). Each Src was subcloned into the pIM2 vector to indicate transfection by mCherry fluorescence. All indicated point mutations were also made using the Agilent kit. The YoPH phosphatase for SrcCD purification was purchased from addgene (79749).

Cell Culture and Transfection

Human embryonic kidney (HEK293) cells and CHO cells were cultured in growth medium supplemented with 10%FBS and incubated at 5% CO_2 and 37˚C. For patch experiments, cells were plated onto 12mm glass coverslips washed in PBS, then ~24 hours later transfected using FuGENE6 (Promega) according to the manufacturer's instructions. Electrophysiological recordings were performed 24-48 hours after transfection.

Electrophysiology

All experiments were performed with an Axopatch 200B patch clamp amplifier, Digidata 1440A digitizer, an Axon CV-203B0 headstage and recorded using pClamp10 software. A Nikon

Intensilight C-HGFI fluorescence lamp was used to visualize successfully transfected cells. Recordings were sampled at 10kHz and filtered to 2kHz prior to analysis. Glass micropipettes (1.5OD, 0.86ID, 75L, Harvard Apparatus) were pulled (P-1000, Sutter Instruments) and fire polished (MF-200 Microforge), yielding 1.5-4MO pipettes for inside-out and whole-cell patches. For all whole-cell recordings, the bath solution contained (in mM) 147 NaCl, 2KCl, 2 $CaCl_2$, 1 $MgCl_2$, 10 HEPES, and 13 Glucose adjusted to pH 7.3 using NaOH. Whole-cell patch pipette solution contained (in mM) 147 NaCl, 10 HEPES, and 10 EGTA adjusted to pH 7.0 using NaOH. For inside-out recordings, both the bath and the pipette solution contained the above whole-cell bath solution except where indicated in text.

c-Src kinase catalytic domain purification

The catalytic domain of Src kinase was purified according to a protocol adapted from an established protocol from another lab[154]. The catalytic domain of *gallus gallus* C-Src (AA251-533, SrcCD) was subcloned into a pNNG vector (ampicillin resistance, T7 promoter), resulting in an N-terminal 8-His tag to the construct. The YopH phosphatase gene encoding amino acids 164-468 contained in a pET-13SA (spectinomycin resistance, T7 promoter) was used to rescue the toxicity of expressing SrcCD in bacterial cells. BL21 cells were co-transformed with pNNG-SrcCD and Pet13SA–YopH phosphatase onto ampicillin (100ug/mL) and spectinomycin (50ug/mL) plates. Colonies were grown O/N in 200mL cultures and then grown to OD ~1.2, then cooled down at 18C for 1hr before inducing with 0.2mM ITPG O/N at 18C. Cells were then harvested by centrifugation at 4C, 4000rpm for 20 minutes and washed once in PBS. After resuspension ((mM) 50 HEPES, 500 NaCl, 10% glycerol, pH 8.0), cells were lysed by 3 cycles of sonication (70% Amplitude, 0.5s on/1.5s off, 30sec), then 0.1mg/mL DNAse and 10mM $MgCl_2$ was added for 10 minutes. The lysate was then centrifuged for 40 minutes at 50,000g, 4C to remove cell debris and insoluble protein. The clarified lysate was mixed with 2mL nickel resin for 2 hours then loaded onto a gravity column, washed ((mM) 50 Tris, 150 NaCl, 40 imidazole, 10%

glycerol, pH 8) then eluted (wash buffer with 400mM imidazole). Samples were further purified by SEC into TBS + 10% glycerol. Fractions were analyzed by SDS page and then pooled and concentrated to 3-6mg/mL. Sample was either stored at 4C for a few weeks or flash frozen and stored at -80C.

Phosphatase PTP1B purification

The tyrosine phosphatase PTP1B (addgene:8601) was subcloned into the pNNG vector, then grown in ampicillin (100ug/mL) and purified as described above for SrcCD. Instead of SEC, buffer was exchanged for TBS + 10% glycerol by serially concentrating and diluting for a final dilution of ~1000X.

KinEASE Assay to measure SrcCD Activity

The KinEASE assay is a time-resolved FRET-based (HTRF) reporter assay which gives a FRET signal that is a function of the proportion of tyrosine kinase substrate that is phosphorylated in a sample. A biotinylated peptide substrate is mixed with a kinase and ATP. The reaction is quenched with the addition of EDTA, as well as two fluorescently conjugated antibodies: one which binds to the biotin tag and the other which only binds to the phosphorylated version of the substrate. When both are bound, they are at a distance from each other such that FRET occurs. Thus, the increase in FRET signal is a function of the proportion of phosphorylated substrate, indicated by the increase in fluorescence emission for the acceptor (650nm) versus the donor (620nm). This was used to measure the kinetic activity of SrcCD and compare it to a commercially purchased full-length Src kinase routinely used for in vitro experiments (Src kinase, active, EMD Millipore). The assay was performed according to the manufacturers instructions. HTRF measurements were performed with the Synergy 2 plate reader (BioTek instruments), with excitation filter 340(30), and emission filters 620(10) and 665(10).

Inside-Out Patch Protocol and Kinase protocol

Inside-out patches were obtained by brief air exposure of patches pulled from Panx1-expressing cells. Voltage steps from -110mV to +110mV was used to confirm presence of Panx1 channels in the patch. Patches were then held at either +70mV, or -40mV until a steady-state amplitude was reached, then perfused for the indicated time with ~5uM SrcCD or ~5uM PTP1B in kinase buffer ((in mM) 150 NaCl, 10 HEPES, 2 $MgCl_2$, and .1 EGTA, pH 7.0). CBX was used to confirm that the residual current was mediated by Panx1. Kinase was activated by incubation with 2mM ATP and 4mM $MgCl_2$ at 4C from 30-60 minutes prior to use.

Results

Phosphomimetic point mutations at Y199 and Y309 generate active Panx1 channels

Panx1 is 'silent' in HEK293 cells, which in the pannexin field, generally means that it generates little to no basal currents near resting membrane potential (typically -10 to -70mV depending on the cell type), nor can it be opened by positive membrane voltages or other means. Any stimulus or modification to the channel that increases its basal and/or evoked currents is said to have 'activated' the channel. It is generally assumed that this gain in function reflects a physiologically relevant transition of the channel to a state where it is capable of fulfilling its role in cell signaling. Thus, HEK293 cells provide a useful platform to study Panx1 channel activation.

To test the hypothesis that Panx1 is a phosphorylation-activated channel, we expressed Panx1 in HEK293 cells with either c-Src or v-Src kinase, respectively the normal and constitutively active forms of the major Src kinase found to phosphorylate Panx1 at Y199 and Y309[35]. But co-expression generated no increase in whole-cell currents as measured by voltage clamp (Figure 1A). Taking an alternative approach, I also performed a 'phosphomimetic' amino acid substitution of tyrosine for aspartate, which generates an increase in local charge density reminiscent of the addition of phosphate to tyrosine. The mutations Y199D and Y309D each produced a channel with leak currents and robust voltage activated currents at positive membrane potentials (Figure 1B). Strikingly, the cells expressing Y309D were mostly dead by ~12 hours after expression. Cells expressing Y199D were mostly dead ~48 hours after expression. This mirrors the effect of overexpressing the caspase-cleaved form of Panx1, which is cytotoxic ostensibly due to the constitutive leakage of cellular metabolites such as ATP.

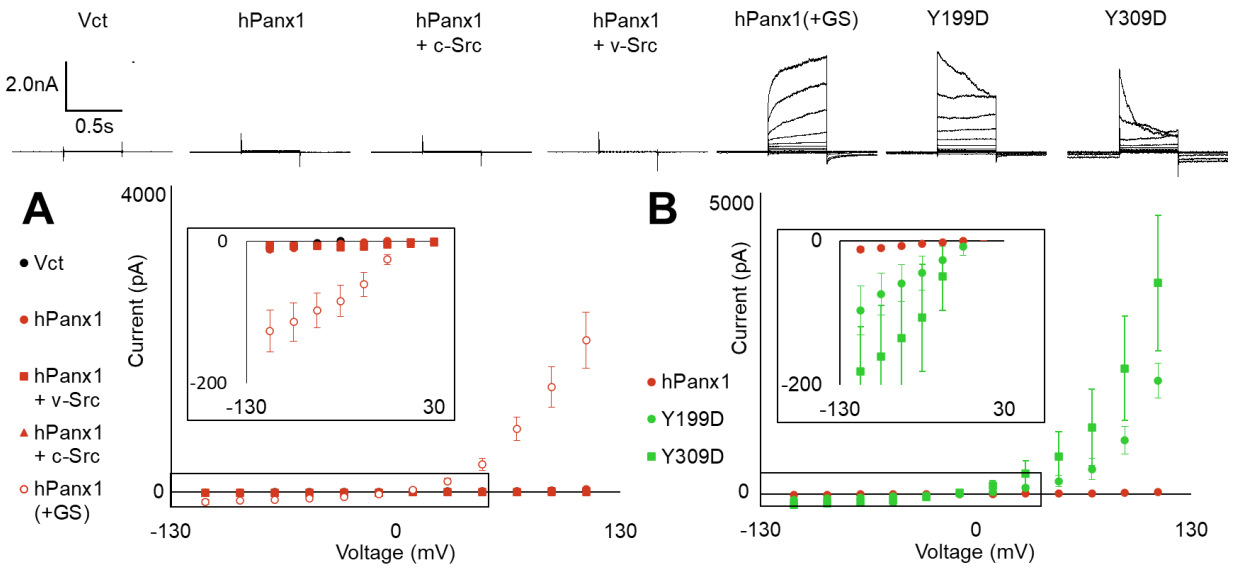

Figure 1. (Top) Exemplar whole-cell patch currents generated from HEK293 cells expressing the indicated constructs. Patches were stepped from -110mV to + 110mV in increments of 20mV, at a holding potential of -70mV. Scale bar indicates the current (nA) travelling through the patch for each 0.5s voltage pulse. **(A)** Quantification of currents from cells expressing hPanx1 alone or in combination with src kinase (c-Src) or its constitutively active variant (v-Src). hPanx1(+GS) is a hyperactivating mutant we previously characterized, which served as a positive control. **(B)** Quantification of currents from hPanx1 and two phosphomimetic point mutations hPanx1 Y199D and Y309D.

Src kinase co-expression and scanning mutagenesis reveal a potential dominant negative phosphoregulatory tyrosine

Given that co-expression failed to activate Panx1, I wondered if over-expression of v-Src may simultaneously suppress Panx1 activity through a different modification to the channel. In support of this idea, co-expression with v-Src abolished the activating effect of Y199D, though not Y309D (Figure 2A). It is possible that an additional tyrosine mediates this suppressing effect. To test this, I mutated each of the 9 cytoplasmic mimic phosphorylation (Y→D) or dephosphorylation (Y→F) (Figure 2B) and assessed the activity of each mutant channel by whole-cell patch clamp. I found that the mutants Y10F, Y150F, and Y150D effected a similar change to Y199D or Y309D (Figure 2C). Interestingly, Y10 and Y150 are also predicted to be substrates for Src family kinases.

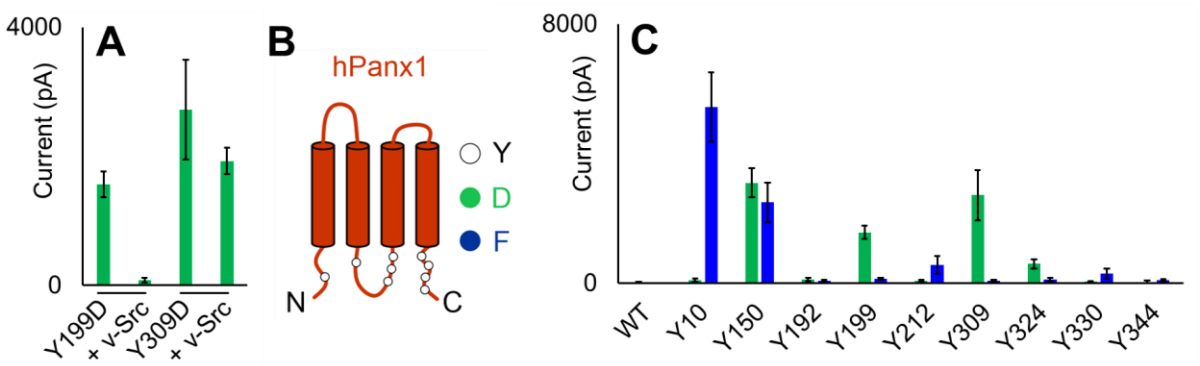

Figure 2. Src-mediated suppression of hPanx1 activity is possibly mediated through other tyrosines. **(A)** Peak currents at +110mV from Y199D or Y309 with or without v-Src co-expression. **(B)** Location of hPanx1 cytoplasmic tyrosines. **(C)** Peak currents obtained from the indicated hPanx1 point mutants.

Since Y10F, but not Y10D, generated an activated Panx1 channel, I focused on this residue as a channel inactivating phosphoregulatory tyrosine. To study the isolated effect of this residue, I first generated a 'maximally-dephosphorylated' Panx1 construct with all 9 tyrosines mutated to phenylalanine, Panx1 9F (Fig 3A). In agreement with the effect of the individual mutants, Panx1 9F is highly active (Figure 3B). These currents are also insensitive to co-expression with v-Src. Restoring Y10 in this construct back to tyrosine (8F Y10) decreased currents, an effect that was amplified by the co-expression of v-Src (Figure 3B). This effect was not observed for 8F Y150, indicating the specificity of this effect for Y10. These data demonstrate that Y10 mediates the suppressive effect of Src kinase co-expression on Panx1 activity, indicating it may be a previously unappreciated phosphoregulatory site.

To assess if the effect at Y10 is dominant, I added the Y10D mutation to the highly active constructs 8F Y10, Y199D and Y309D (Figure 3A,C). All of these constructs yielded tiny whole-cell currents compared to the parent construct with Y10 intact. The effect of Y10D is most likely not due to improper folding or trafficking, as Panx1 Y10D expresses well and folds properly (Figure 3D). Together, these data suggest that Panx1 may have a master regulatory switch at Y10 which, when phosphorylated, keeps the channel inactive.

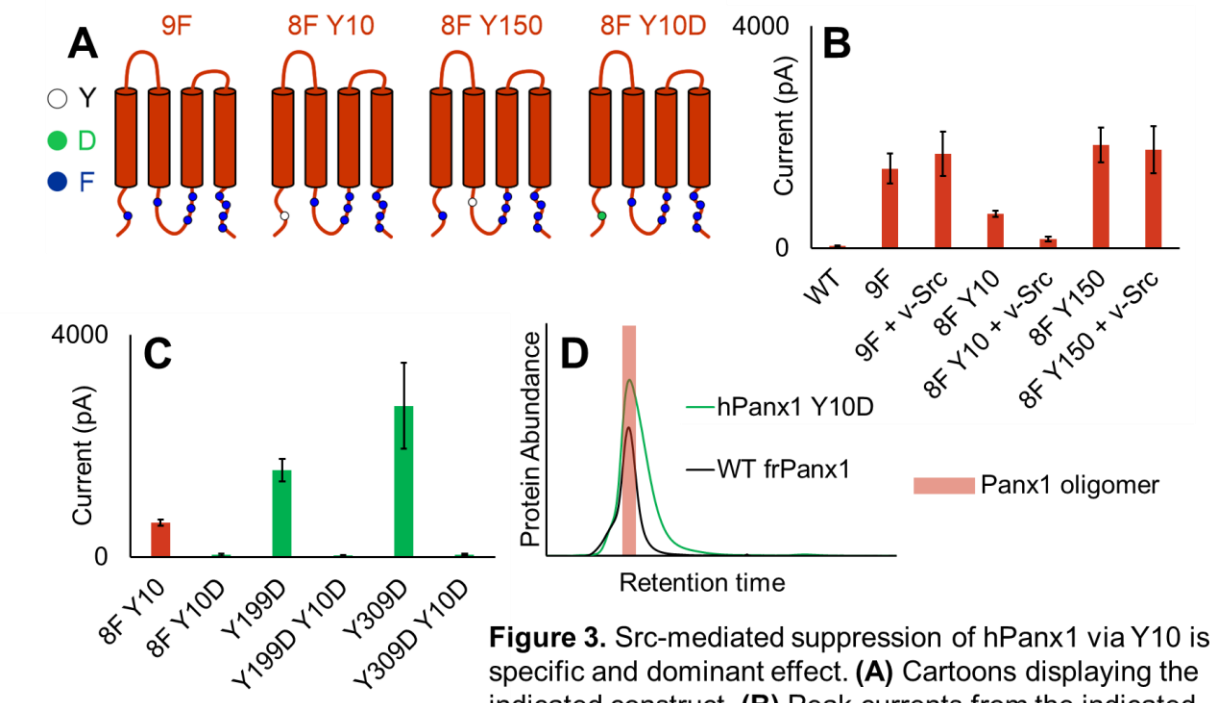

Figure 3. Src-mediated suppression of hPanx1 via Y10 is a specific and dominant effect. **(A)** Cartoons displaying the indicated construct. **(B)** Peak currents from the indicated construct with or without v-Src co-expression. **(C)** Peak currents obtained from the indicated constructs. **(D)** Representative SEC chromatograms of hPanx1 Y10D and the stable, well-folded WT frPanx1 used routinely for structural studies.

Src kinase does not modulate Panx1 in inside-out patches

I then sought to determine if Src kinase could shut Panx1 8F Y10 channels in real time by perfusing Src onto the cytoplasmic side of an inside-out membrane patch (Figure 4A). I first purified the catalytic domain of c-Src kinase (SrcCD), which has previously been shown to have high activity and limited preference for tyrosine kinase substrates[154]. I then tested the catalytic activity of SrcCD with the KinEASE (Cisbio, France) time-resolved FRET (HTRF) assay (see methods for details). The activity of SrcCD was compared to a commercially available full-length active Src kinase (EMD Millipore) by an enzyme titration experiment. The SrcCD converted substrate with a ~30x higher specific activity than the commercially available kinase, in agreement with the existing literature.

After pulling inside-out patches from HEK cells expressing hPanx1 8F Y10 and confirming channel activity using voltage steps, I applied SrcCD at both resting membrane potential and a

depolarizing potential. As shown, SrcCD perfusion had little to no effect on steady state currents (Figure 4B), and little effect on voltage steps (Figure 4C). I also attempted to perfuse a tyrosine phosphatase (PTP1B) onto the wild-type channel, reasoning that if Y10 is basally phosphorylated in HEK293 cells, then dephosphorylation by PTP1B may be able to activate Panx1. No change in currents were observed (Figure 4D). I also applied SrcCD to the wild-type channel, reasoning that if Y10-mediated suppression of Panx1 currents only occurs in live cells, then perhaps activation through Y199 or Y309 could be resolved. It is known that these residues are phosphorylated in vitro by Src[35]. Once again, SrcCD failed to increase currents (Figure 4D).

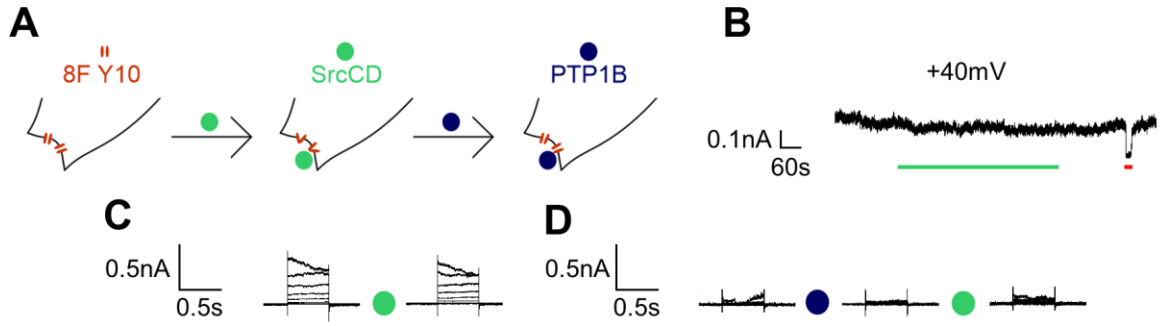

Figure 4. Tyrosine kinase and phosphatase treatment do not modulate Panx1 in inside-out patches. **(A)** Cartoon displaying the application of SrcCD or PTP1B to the cytoplasmic side of 8F Y10 and the expected outcome on channel opening or closure. **(B)** 5-min Application of SrcCD (green bar) to open Panx1 8F Y10 channels. The inhibitor CBX (red bar) was used to confirm currents were carried by Panx1. **(C)** Voltage steps before and after 5 minute application of SrcCD (green dot) to an 8F Y10 inside-out patch near resting membrane potential (-70mV) . **(D)** 5-min application of PTP1B (blue dot) or SrcCD to WT hPanx1.

Discussion

We investigated the possibility of Panx1 gating by phosphorylation and found support for activation and deactivation of the channel by phosphorylation at different cytoplasmic tyrosines. In particular, we discovered a novel potential negative regulation of Panx1 by phosphorylation at Y10. This could explain why Panx1 is inactive when expressed in various mammalian cell types but not others. However, we failed to establish that tyrosine phosphorylation at Y10 or any other tyrosine alone is sufficient to activate or inactivate the channel. One important note is that

irreversible run-up of Panx1 currents was often observed in inside out patches, regardless of the construct used (Figure 5). This does not occur in Panx1 channels recorded from whole-cell patches. Altered behavior in excised patches is common for many ion channels, which is perhaps unsurprising given their high mechanical tensions, altered membrane composition, and disrupted cytoskeletal networks. Thus, this extreme environment may cause Panx1 to shed some of its natural regulatory mechanisms such as Y10 mediated inactivation.

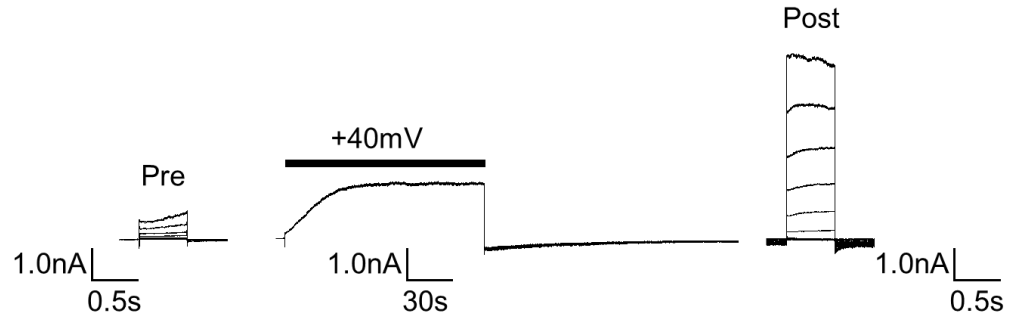

Figure 5. Irreversible run-up of Panx1 8F Y10 currents in inside-out patches. Voltage steps before (Pre) and after (Post) a 2-minute step to +40mV of an inside out patch of pulled from HEK293 cells expressing Panx1 8F Y10.

Future work could involve performing Panx1 immunoblots to see if hPanx1 phosphorylation at Y10 increases following Src kinase co-expression. Additionally, it would be interesting to see if simply adding Src kinase to the whole-cell patch pipette could cause inactivation of Panx1 over the course of a few minutes after establishing whole-cell configuration. These data could at least further support that Y10 is indeed a phosphoregulatory site. Alternatively, if phosphorylation at Y10 does not occur, then other N-terminal PTMs may be responsible for Src-mediated inactivation. Indeed, N-terminal acetylation of Panx1 in breast cancer cells has recently been reported[155]. On the other hand, they did not find evidence of Y10 phosphorylation, but the channel was also active in this cancer cell type.

REFERENCES

1. Pelegrin, P. *Purinergic Signaling*. *Methods in Molecular Biology* **2041**, (2020).

2. North, R. A. Molecular physiology of P2X receptors. *Physiol. Rev.* **82**, 1013–1067 (2002).

3. Pankratov, Y., Lalo, U., Krishtal, O. A. & Verkhratsky, A. P2X receptors and synaptic plasticity. *Neuroscience* **158**, 137–148 (2009).

4. Kolen, K. & Slegers, H. Integration of P2Y receptor-activated signal transduction pathways in G protein-dependent signalling networks. *Purinergic Signal.* **2**, 451–469 (2006).

5. Borea, P. A., Gessi, S., Merighi, S., Vincenzi, F. & Varani, K. Pharmacology of adenosine receptors: The state of the art. *Physiol. Rev.* **98**, 1591–1625 (2018).

6. Moriyama, Y., Hiasa, M., Sakamoto, S., Omote, H. & Nomura, M. Vesicular nucleotide transporter (VNUT): appearance of an actress on the stage of purinergic signaling. *Purinergic Signal.* **13**, 387–404 (2017).

7. Taruno, A. ATP release channels. *Int. J. Mol. Sci.* **19**, (2018).

8. Syrjanen, J., Michalski, K., Kawate, T. & Furukawa, H. On the molecular nature of large-pore channels. *J. Mol. Biol.* **433**, 166994 (2021).

9. Panchina, Y. *et al.* A ubiquitous family of putative gap junction molecules. *Curr. Biol.* **10**, 473–474 (2000).

10. Medina, C. B. *et al.* Metabolites released from apoptotic cells act as tissue messengers. *Nature* **580**, 1–6 (2020).

11. O'Donnell, B. L. & Penuela, S. Pannexin 3 channels in health and disease. *Purinergic Signal.* **17**, 577–589 (2021).

12. Labra, V. C. *et al.* The Neuroglial Dialog Between Cannabinoids and Hemichannels. *Front. Mol. Neurosci.* **11**, 1–17 (2018).

13. Li, S. *et al.* Expression and roles of pannexins in ATP release in the pituitary gland. *Endocrinology* **152**, 2342–2352 (2011).

14. Penuela, S., Gehi, R. & Laird, D. W. The biochemistry and function of pannexin channels. *Biochim. Biophys. Acta - Biomembr.* **1828**, 15–22 (2013).

15. Chiu, Y. H., Schappe, M. S., Desai, B. N. & Bayliss, D. A. Revisiting multimodal activation and channel properties of Pannexin 1. *J. Gen. Physiol.* **150**, 19–39 (2018).

16. Mim, C., Perkins, G. & Dahl, G. Structure versus function: Are new conformations of pannexin 1 yet to be resolved? *J. Gen. Physiol.* **153**, 1–17 (2021).

17. Idzko, M., Ferrari, D. & Eltzschig, H. K. Nucleotide signalling during inflammation. *Nature* **509**, 310–317 (2014).

18. Harcha, P. A., López-López, T., Palacios, A. G. & Sáez, P. J. Pannexin Channel Regulation of Cell Migration: Focus on Immune Cells. *Front. Immunol.* **12**, 1–15 (2021).

19. Chekeni, F. B. *et al.* Pannexin 1 channels mediate 'find-me' signal release and membrane permeability during apoptosis. *Nature* **467**, 863–867 (2010).

20. Dosch, M., Gerber, J., Jebbawi, F. & Beldi, G. Mechanisms of ATP release by inflammatory cells. *Int. J. Mol. Sci.* **19**, 1–16 (2018).

21. Bao, Y., Chen, Y., Ledderose, C., Li, L. & Junger, W. G. Pannexin 1 channels link chemoattractant receptor signaling to local excitation and global inhibition responses at the front and back of polarized neutrophils. *J. Biol. Chem.* **288**, 22650–22657 (2013).

22. Thorstenberg, M. L. *et al.* Purinergic cooperation between P2Y2 and P2X7 receptors

promote cutaneous leishmaniasis control: Involvement of pannexin-1 and leukotrienes. *Front. Immunol.* **9**, (2018).

23. Lohman, A. W. *et al.* Pannexin 1 channels regulate leukocyte emigration through the venous endothelium during acute inflammation. *Nat. Commun.* **6**, 1–12 (2015).

24. Moore, K. J., Sheedy, F. J. & Fisher, E. A. Macrophages in atherosclerosis: A dynamic balance. *Nat. Rev. Immunol.* **13**, 709–721 (2013).

25. Molica, F. *et al.* Pannexin1 links lymphatic function to lipid metabolism and atherosclerosis. *Sci. Rep.* **7**, 1–12 (2017).

26. Medina, C. B. *et al.* Pannexin 1 channels facilitate communication between T cells to restrict the severity of airway inflammation. *Immunity* **54**, 1715-1727.e7 (2021).

27. Filiberto, A. C. *et al.* Endothelial pannexin-1 channels modulate macrophage and smooth muscle cell activation in abdominal aortic aneurysm formation. *Nat. Commun.* **13**, 1–11 (2022).

28. Burnstock, G. Purinergic Signaling in the Cardiovascular System. *Circ. Res.* **120**, 207–228 (2017).

29. Billaud, M. *et al.* Pannexin1 regulates α1-adrenergic receptor- mediated vasoconstriction. *Circ. Res.* **109**, 80–85 (2011).

30. Billaud, M. *et al.* A molecular signature in the pannexin1 intracellular loop confers channel activation by the α1 adrenoreceptor in smooth muscle cells. *Sci. Signal.* **8**, 1–13 (2015).

31. Good, M. E. *et al.* Pannexin 1 channels as an unexpected new target of the anti-hypertensive drug spironolactone. *Circ. Res.* **122**, 606–615 (2018).

32. DeLalio, L. J. *et al.* Interaction between pannexin 1 and caveolin-1 in smooth muscle can

regulate blood pressure. *Arterioscler. Thromb. Vasc. Biol.* **38**, 2065–2078 (2018).

33. Grimmer, B. *et al.* Pannexin 1 – a novel regulator of hypoxic pulmonary vasoconstriction. *FASEB J.* **35**, 1–13 (2021).

34. Billaud, M. *et al.* A molecular signature in the pannexin1 intracellular loop confers channel activation by the α1 adrenoreceptor in smooth muscle cells. *Sci. Signal.* **8**, 1–13 (2015).

35. DeLalio, L. J. *et al.* Constitutive SRC-mediated phosphorylation of pannexin 1 at tyrosine 198 occurs at the plasma membrane. *J. Biol. Chem.* **294**, 6940–6956 (2019).

36. Gaynullina, D., Tarasova, O. S., Kiryukhina, O. O., Shestopalov, V. I. & Panchin, Y. Endothelial function is impaired in conduit arteries of pannexin1 knockout mice. *Biol. Direct* **9**, 1–5 (2014).

37. Wang, S. P. *et al.* Endothelial cation channel PIEZO1 controls blood pressure by mediating flow-induced ATP release. *J. Clin. Invest.* **126**, 4527–4536 (2016).

38. Daneva, Z. *et al.* Endothelial pannexin 1–trpv4 channel signaling lowers pulmonary arterial pressure in mice. *Elife* **10**, 1–26 (2021).

39. Bisht, K. *et al.* Capillary-associated microglia regulate vascular structure and function through PANX1-P2RY12 coupling in mice. *Nat. Commun.* **12**, (2021).

40. Adamson, S. E. *et al.* Pannexin 1 is required for full activation of insulin-stimulated glucose uptake in adipocytes. *Mol. Metab.* **4**, 610–618 (2015).

41. Lee, V. R. *et al.* Pannexin 1 regulates adipose stromal cell differentiation and fat accumulation. *Sci. Rep.* **8**, 1–14 (2018).

42. Tozzi, M., Hansen, J. B. & Novak, I. Pannexin-1 mediated ATP release in adipocytes is sensitive to glucose and insulin and modulates lipolysis and macrophage migration. *Acta*

Physiol. **228**, 1–19 (2020).

43. Wakefield, C. B. *et al.* Pannexin 3 deletion reduces fat accumulation and inflammation in a sex-specific manner. *Int. J. Obes.* **46**, 726–738 (2022).

44. Sanchez-Arias, J. C. *et al.* Purinergic signaling in nervous system health and disease: Focus on pannexin 1. *Pharmacol. Ther.* **225**, 107840 (2021).

45. Gajardo, I. *et al.* Lack of pannexin 1 alters synaptic GluN2 subunit composition and spatial reversal learning in mice. *Front. Mol. Neurosci.* **11**, 1–14 (2018).

46. Sanchez-Arias, J. C. *et al.* Pannexin 1 regulates network ensembles and dendritic spine development in cortical neurons. *eNeuro* **6**, (2019).

47. Chen, J., Liang, C., Zong, L., Zhu, Y. & Zhao, H. B. Knockout of pannexin-1 induces hearing loss. *Int. J. Mol. Sci.* **19**, 1–11 (2018).

48. Ishikawa, M. & Yamada, Y. The Role of Pannexin 3 in Bone Biology. *J. Dent. Res.* **96**, 372–379 (2017).

49. Koval, M. *et al.* Pannexin 1 as a driver of inflammation and ischemia–reperfusion injury. *Purinergic Signal.* **17**, 521–531 (2021).

50. Muñoz, M. F., Griffith, T. N. & Contreras, J. E. Mechanisms of ATP release in pain: role of pannexin and connexin channels. *Purinergic Signalling* **17**, 549–561 (2021).

51. Engelhardt, K., Schmidt, M., Tenbusch, M. & Dermietzel, R. Effects on Channel Properties and Induction of Cell Death Induced by C-terminal Truncations of Pannexin1 Depend on Domain Length. *J. Membr. Biol.* **248**, 285–294 (2015).

52. Chiu, Y. H. *et al.* Deacetylation as a receptor-regulated direct activation switch for pannexin channels. *Nat. Commun.* **12**, 1–14 (2021).

53. Sandilos, J. K. *et al.* Pannexin 1, an ATP release channel, is activated by caspase cleavage of its pore-associated C-terminal autoinhibitory region. *J. Biol. Chem.* **287**, 11303–11311 (2012).

54. Jin, X. *et al.* A constitutively closed pannexin1 channel in lipid bilayer nanodiscs assembles as a large-pore heptamer. *bioRxiv* (2021). doi:10.1101/2020.12.31.425019

55. Ruan, Z., Orozco, I. J., Du, J. & Lü, W. Structures of human pannexin 1 reveal ion pathways and mechanism of gating. *Nature* **584**, 646–651 (2020).

56. Wang, J. & Dahl, G. Pannexin1: A multifunction and multiconductance and/or permeability membrane channel. *Am. J. Physiol. - Cell Physiol.* **315**, C290–C299 (2018).

57. Mou, L. *et al.* Structural basis for gating mechanism of Pannexin 1 channel. *Cell Res.* **30**, 452–454 (2020).

58. Narahari, A. K. *et al.* Atp and large signaling metabolites flux through caspase-activated pannexin 1 channels. *Elife* **10**, 1–21 (2021).

59. Bruzzone, R., Hormuzdi, S. G., Barbe, M. T., Herb, A. & Monyer, H. Pannexins, a family of gap junction proteins expressed in brain. *Proc. Natl. Acad. Sci.* **100**, 13644–13649 (2003).

60. Harris, A. L. *Emerging issues of connexin channels: Biophysics fills the gap*. *Quarterly Reviews of Biophysics* **34**, (2001).

61. Romanov, R. A. *et al.* The ATP permeability of pannexin 1 channels in a heterologous system and in mammalian taste cells is dispensable. *J. Cell Sci.* **125**, 5514–5523 (2012).

62. Nomura, T. *et al.* Current-direction/amplitude-dependent single channel gating kinetics of mouse pannexin 1 channel: A new concept for gating kinetics. *Sci. Rep.* **7**, 1–13 (2017).

63. Michalski, K., Henze, E., Nguyen, P., Lynch, P. & Kawate, T. The weak voltage dependence of pannexin 1 channels can be tuned by N-terminal modifications. 1–11 (2018).

64. Ambrosi, C. *et al.* Pannexin1 and pannexin2 channels show quaternary similarities to connexons and different oligomerization numbers from each other. *J. Biol. Chem.* **285**, 24420–24431 (2010).

65. Poon, I. K. H. *et al.* Unexpected link between an antibiotic, pannexin channels and apoptosis. *Nature* **507**, 329–334 (2014).

66. Bao, L., Locovei, S. & Dahl, G. Pannexin membrane channels are mechanosensitive conduits for ATP. *FEBS Lett.* **572**, 65–68 (2004).

67. Locovei, S., Bao, L. & Dahl, G. Pannexin 1 in erythrocytes: Function without a gap. *Proc. Natl. Acad. Sci. U. S. A.* **103**, 7655–7659 (2006).

68. Jiang, Y., Yang, X., Jiang, J. & Xiao, B. Structural Designs and Mechanogating Mechanisms of the Mechanosensitive Piezo Channels. *Trends Biochem. Sci.* **46**, 472–488 (2021).

69. Desplat, A. *et al.* Piezo1-Pannexin1 complex couples force detection to ATP secretion in cholangiocytes. *J. Gen. Physiol.* **153**, (2021).

70. Diem, K. *et al.* Mechanical stretch activates piezo1 in caveolae of alveolar type I cells to trigger ATP release and paracrine stimulation of surfactant secretion from alveolar type II cells. *FASEB J.* **34**, 12785–12804 (2020).

71. Cinar, E. *et al.* Piezo1 regulates mechanotransductive release of ATP from human RBCs. *Proc. Natl. Acad. Sci. U. S. A.* **112**, 11783–11788 (2015).

72. López, X. *et al.* A physiologic rise in cytoplasmic calcium ion signal increases pannexin1

channel activity via a C-terminus phosphorylation by CaMKII. *Proc. Natl. Acad. Sci. U. S. A.* **118**, 1–10 (2021).

73. Sangaletti, R., Dahl, G. & Bianchi, L. Mechanosensitive unpaired innexin channels in C. elegans touch neurons. *Am. J. Physiol. - Cell Physiol.* **307**, C966–C977 (2014).

74. Walker, D. S. & Schafer, W. R. Distinct roles for innexin gap junctions and hemichannels in mechanosensation. *Elife* **9**, 1–21 (2020).

75. Silverman, W. R. *et al.* The pannexin 1 channel activates the inflammasome in neurons and astrocytes. *J. Biol. Chem.* **284**, 18143–18151 (2009).

76. Deng, Z. *et al.* Cryo-EM structures of the ATP release channel pannexin 1. *Nat. Struct. Mol. Biol.* **27**, 373–381 (2020).

77. Jin, Q. *et al.* Cryo-EM structures of human pannexin 1 channel. *Cell Research* **30**, 449–451 (2020).

78. Michalski, K. & Kawate, T. Carbenoxolone inhibits Pannexin1 channels through interactions in the first extracellular loop. *J. Gen. Physiol.* **147**, 165–174 (2016).

79. Locovei, S., Wang, J. & Dahl, G. Activation of pannexin 1 channels by ATP through P2Y receptors and by cytoplasmic calcium. *FEBS Lett.* **580**, 239–244 (2006).

80. Weilinger, N. L., Tang, P. L. & Thompson, R. J. Anoxia-induced NMDA receptor activation opens Pannexin channels via Src family kinases. *J. Neurosci.* **32**, 12579–12588 (2012).

81. Weilinger, N. L. *et al.* Metabotropic NMDA receptor signaling couples Src family kinases to pannexin-1 during excitotoxicity. *Nat. Neurosci.* **19**, 432–442 (2016).

82. Imamura, H., Sakamoto, S., Yoshida, T. & Matsui, Y. Single-cell dynamics of pannexin-1-

facilitated programmed ATP loss during apoptosis. *Elife* 1–20 (2020).

83. Wang, J. & Dahl, G. SCAM analysis of Panx1 suggests a peculiar pore structure. *J. Gen. Physiol.* **136**, 515–527 (2010).

84. Zhang, S. *et al.* Structure of the full-length human Pannexin1 channel and insights into its role in pyroptosis. *Cell Discov.* **7**, (2021).

85. Michalski, K. *et al.* The Cryo-EM structure of pannexin 1 reveals unique motifs for ion selection and inhibition. *Elife* **9**, 1–14 (2020).

86. Kuang, Y. P. A pannexin 1 channelopathy causes human oocyte death. *Sci. Transl. Med.* **39**, 443–445 (2019).

87. Kuzuya, M. *et al.* Structures of human pannexin-1 in nanodiscs reveal gating mediated by dynamic movement of the N terminus and phospholipids. *Sci. Signal.* **15**, eabg6941 (2022).

88. Lohman, A. W. *et al.* S-nitrosylation inhibits pannexin 1 channel function. *J. Biol. Chem.* **287**, 39602–39612 (2012).

89. Oishi, S. *et al.* Stretch of atrial myocytes stimulates recruitment of macrophages via ATP released through gap-junction channels. *J. Pharmacol. Sci.* **120**, 296–304 (2012).

90. Good, M. E. *et al.* Emerging concepts regarding pannexin 1 in the vasculature. *Biochem. Soc. Trans.* **43**, 495–501 (2015).

91. Yeung, A. K., Patil, C. S. & Jackson, M. F. Pannexin-1 in the CNS: Emerging concepts in health and disease. *J. Neurochem.* **154**, 468–485 (2020).

92. Senthivinayagam, S. *et al.* Adaptive thermogenesis in brown adipose tissue involves activation of pannexin-1 channels. *Mol. Metab.* **44**, 101130 (2021).

93. Berchtold, L. A. *et al.* Pannexin-2-deficiency sensitizes pancreatic β-cells to cytokine-induced apoptosis in vitro and impairs glucose tolerance in vivo. *Mol. Cell. Endocrinol.* **448**, 108–121 (2017).

94. Tozzi, M. *et al.* The P2X7 receptor and pannexin-1 are involved in glucose-induced autocrine regulation in β-cells. *Sci. Rep.* **8**, 1–15 (2018).

95. Bargiotas, P. *et al.* Pannexins in ischemia-induced neurodegeneration. *Proc. Natl. Acad. Sci. U. S. A.* **108**, 20772–20777 (2011).

96. Muñoz, M. F., Griffith, T. N. & Contreras, J. E. Mechanisms of ATP release in pain: role of pannexin and connexin channels. *Purinergic Signal.* **17**, 549–561 (2021).

97. Ma, W., Hui, H., Pelegrin, P. & Surprenant, A. Pharmacological characterization of pannexin-1 currents expressed in mammalian cells. *J. Pharmacol. Exp. Ther.* **328**, 409–418 (2009).

98. Galietta, L. J. V, Haggie, P. M. & Verkman, A. S. Green fluorescent protein-based halide indicators with improved chloride and iodide affinities. *FEBS Lett.* **499**, 220–224 (2001).

99. Karasawa, A. & Kawate, T. Structural basis for subtype-specific inhibition of the P2X7 receptor. *Elife* **5**, 1–17 (2016).

100. Karasawa, A. & Kawate, T. Expression and Purification of a Mammalian P2X7 Receptor from Sf9 Insect Cells. *Bio-Protocol* **7**, 1–16 (2017).

101. Chambers, M. C. *et al.* A cross-platform toolkit for mass spectrometry and proteomics. *Nat. Biotechnol.* **30**, 918–920 (2012).

102. Helf, M. J., Fox, B. W., Artyukhin, A. B., Zhang, Y. K. & Schroeder, F. C. Comparative metabolomics with Metaboseek reveals functions of a conserved fat metabolism pathway in C. elegans. *Nat. Commun.* **13**, 1–11 (2022).

103. Karasawa, A., Michalski, K., Mikhelzon, P. & Kawate, T. The P2X7 receptor forms a dye-permeable pore independent of its intracellular domain but dependent on membrane lipid composition. *Elife* **6**, 1–22 (2017).

104. Quehenberger, O. *et al.* Lipidomics reveals a remarkable diversity of lipids in human plasma1. *J. Lipid Res.* **51**, 3299–3305 (2010).

105. Ma, W. *et al.* Pannexin 1 forms an anion-selective channel. *Pflugers Arch. Eur. J. Physiol.* **463**, 585–592 (2012).

106. Liu, P. *et al.* The mechanisms of lysophosphatidylcholine in the development of diseases. *Life Sci.* **247**, 117443 (2020).

107. Galietta, L. J. V., Haggie, P. M. & Verkman, A. S. Green fluorescent protein-based halide indicators with improved chloride and iodide affinities. *FEBS Lett.* **499**, 220–224 (2001).

108. Elizabeth M. Leimer, Kirk L. Pappan, Dana L. Nettles, Richard D. Bell, M. E. & Easley, Steven A. Olson, Lori A. Setton, and S. B. A. Lipid Profile of Human Synovial Fluid Following Intra-Articular Ankle Fracture. *Physiol. Behav.* **176**, 100–106 (2016).

109. Hung, C. H. *et al.* Activation of acid-sensing ion channel 3 by lysophosphatidylcholine 16:0 mediates psychological stress-induced fibromyalgia-like pain. *Ann. Rheum. Dis.* **79**, 1644–1656 (2020).

110. Argiolas, A. & Pisano, J. J. Facilitation of phospholipase A2 activity by mastoparans, a new class of mast cell degranulating peptides from wasp venom. *J. Biol. Chem.* **258**, 13697–13702 (1983).

111. Joyce-Brady, M. *et al.* Mechanisms of mastoparan-stimulated surfactant secretion from isolated pulmonary alveolar type 2 cells. *J. Biol. Chem.* **266**, 6859–6865 (1991).

112. Gil, J., Higgins, T. & Rozengurt, E. Mastoparan, a novel mitogen for Swiss 3T3 cells,

stimulates pertussis toxin-sensitive arachidonic acid release without inositol phosphate accumulation. *J. Cell Biol.* **113**, 943–950 (1991).

113. Higashijima, T., Uzu, S., Nakajima, T. & Ross, E. M. Mastoparan, a peptide toxin from wasp venom, mimics receptors by activating GTP-binding regulatory proteins (G proteins). *J. Biol. Chem.* **263**, 6491–6494 (1988).

114. Sukumar, M., Ross, E. M. & Higashijima, T. A G(s)-selective analog of the receptor-mimetic peptide mastoparan binds to G(s)α in a kinked helical conformation. *Biochemistry* **36**, 3632–3639 (1997).

115. Sirianant, L., Ousingsawat, J., Wanitchakool, P., Schreiber, R. & Kunzelmann, K. Cellular volume regulation by anoctamin 6: Ca2+, phospholipase A2 and osmosensing. *Pflugers Arch. Eur. J. Physiol.* **468**, 335–349 (2016).

116. Vanden Abeele, F. *et al.* Ca2+-independent phospholipase A2-dependent gating of TRPM8 by lysophospholipids. *J. Biol. Chem.* **281**, 40174–40182 (2006).

117. De Azevedo, R. A. *et al.* Mastoparan induces apoptosis in B16F10-Nex2 melanoma cells via the intrinsic mitochondrial pathway and displays antitumor activity in vivo. *Peptides* **68**, 113–119 (2015).

118. Rocha, T. *et al.* Inflammation and apoptosis induced by mastoparan Polybia-MPII on skeletal muscle. *Toxicon* **55**, 1213–1221 (2010).

119. Ma, Y. C., Huang, J., Ali, S., Lowry, W. & Huang, X. Y. Src tyrosine kinase is a novel direct effector of G proteins. *Cell* **102**, 635–646 (2000).

120. Law, S. H. *et al.* An updated review of lysophosphatidylcholine metabolism in human diseases. *Int. J. Mol. Sci.* **20**, 1–24 (2019).

121. Zhang, Q. *et al.* Lysophosphatidylcholine promotes intercellular adhesion molecule-1 and

vascular cell adhesion molecule-1 expression in human umbilical vein endothelial cells via an orphan G protein receptor 2-mediated signaling pathway. *Bioengineered* **12**, 4520–4535 (2021).

122. Ismaeel, S. & Qadri, A. ATP Release Drives Inflammation with Lysophosphatidylcholine. *ImmunoHorizons* **5**, 219–233 (2021).

123. Galle, J., Bassenge, E. & Busse, R. Oxidized low density lipoproteins potentiate vasoconstrictions to various agonists by direct interaction with vascular smooth muscle. *Circ. Res.* **66**, 1287–1293 (1990).

124. Galle, J. *et al.* Oxidized LDL and its compound lysophosphatidylcholine potentiate AngII-induced vasoconstriction by stimulation of RhoA. *J. Am. Soc. Nephrol.* **14**, 1471–1479 (2003).

125. Steinbrecher, U. P., Parthasarathy, S., Leake, D. S., Witztum, J. L. & Steinberg, D. Modification of low density lipoprotein by endothelial cells involves lipid peroxidation and degradation of low density lipoprotein phospholipids. *Proc. Natl. Acad. Sci. U. S. A.* **81**, 3883–3887 (1984).

126. Lauber, K. *et al.* Apoptotic cells induce migration of phagocytes via caspase-3-mediated release of a lipid attraction signal. *Cell* **113**, 717–730 (2003).

127. Giera, M. *et al.* Lipid and lipid mediator profiling of human synovial fluid in rheumatoid arthritis patients by means of LC-MS/MS. *Biochim. Biophys. Acta - Mol. Cell Biol. Lipids* **1821**, 1415–1424 (2012).

128. Marra, S. *et al.* Non-acidic activation of pain-related Acid-Sensing Ion Channel 3 by lipids. *EMBO J.* **35**, 414–428 (2016).

129. Janczi, T. *et al.* A novel pro-inflammatory mechanosensing pathway orchestrated by the

disintegrin metalloproteinase adam15 in synovial fibroblasts. *Cells* **10**, (2021).

130. da Silva, J. L. G., Passos, D. F., Bernardes, V. M. & Leal, D. B. R. ATP and adenosine: Role in the immunopathogenesis of rheumatoid arthritis. *Immunol. Lett.* **214**, 55–64 (2019).

131. Makarenkova, H. P. & Shestopalov, V. I. The role of pannexin hemichannels in inflammation and regeneration. *Front. Physiol.* **5 FEB**, 1–8 (2014).

132. Kopp, R., Krautloher, A., Ramírez-Fernández, A. & Nicke, A. P2X7 Interactions and Signaling – Making Head or Tail of It. *Front. Mol. Neurosci.* **12**, 1–25 (2019).

133. Jiang, H. *et al.* Stimulation of rat erythrocyte P2X 7 receptor induces the release of epoxyeicosatrienoic acids. *Br. J. Pharmacol.* **151**, 1033–1040 (2007).

134. Alzola, E. *et al.* Activation by P2X7 agonists of two phospholipases A2 (PLA2) in ductal cells of rat submandibular gland: Coupling of the calcium-independent PLA2 with kallikrein secretion. *J. Biol. Chem.* **273**, 30208–30217 (1998).

135. Janks, L., Sprague, R. S. & Egan, T. M. ATP-Gated P2X7 Receptors Require Chloride Channels To Promote Inflammation in Human Macrophages. *J. Immunol.* **202**, 883–898 (2019).

136. Leoncini, G. & Signorello, M. G. N-ethylmaleimide-stimulated arachidonic acid release in human platelets. *Biochem. Pharmacol.* **57**, 785–791 (1999).

137. McHowat, J. & Creer, M. H. Thrombin activates a membrane-associated calcium-independent PLA2 in ventricular myocytes. *Am. J. Physiol. - Cell Physiol.* **274**, 447–454 (1998).

138. Seminario-Vidal, L. *et al.* Thrombin promotes release of ATP from lung epithelial cells through coordinated activation of Rho- and Ca2+ -dependent signaling pathways. *J. Biol.*

Chem. **284**, 20638–20648 (2009).

139. Gödecke, S. *et al.* Thrombin-induced ATP release from human umbilical vein endothelial cells. *Am. J. Physiol. - Cell Physiol.* **302**, 915–923 (2012).

140. Taylor, K. A., Wright, J. R., Vial, C., Evans, R. J. & Mahaut-Smith, M. P. Amplification of human platelet activation by surface pannexin-1 channels. *J. Thromb. Haemost.* **12**, 987–998 (2014).

141. Scholz-pedretti, K., Gans, A. & Beck, K. Potentiation of TNF- ␣ – Stimulated Group IIA Phospholipase A 2 Expression by Peroxisome Proliferator – Activated Receptor ␣ Activators in Rat Mesangial Cells. 611–620 (2002).

142. Liu, S. J. & McHowat, J. Stimulation of different phospholipase A2 isoforms by TNF-α and IL-1β in adult rat ventricular myocytes. *Am. J. Physiol. - Hear. Circ. Physiol.* **44**, 1462–1472 (1998).

143. Rat, C. & Cells, G. Cytokine-stimulated Secretion of Group 11 Phospholipase A2 by Rat Mesangial Cells Its Contribution to Arachidonic Acid Release and Prostaglandin. **92**, (1993).

144. Tagesson, C., Boll, R. & Kald, B. Tumor Necrosis Factor- α Potentiates Phospholipase A 2 -Stimulated Release and Metabolism of Arachidonic Acid in Cultured Intestinal Epithelial Cells (INT 407) Tumor Necrosis Factor-a Potentiates Phospholipase A , - Stimulated Release and Metabolism of A. **5521**, (2009).

145. Vriens, J. *et al.* Cell swelling, heat, and chemical agonists use distinct pathways for the activation of the cation channel TRPV4. *Proc. Natl. Acad. Sci. U. S. A.* **101**, 396–401 (2004).

146. Peng, S., Poole, D. P. & Veldhuis, N. A. Mini-review: Dissecting receptor-mediated

stimulation of TRPV4 in nociceptive and inflammatory pathways. *Neurosci. Lett.* **770**, 136377 (2022).

147. Batsika, C. S., Gerogiannopoulou, A. D. D., Mantzourani, C., Vasilakaki, S. & Kokotos, G. The design and discovery of phospholipase A2 inhibitors for the treatment of inflammatory diseases. *Expert Opin. Drug Discov.* **16**, 1287–1305 (2021).

148. Chang, W., Hatch, G. M., Wang, Y., Yu, F. & Wang, M. The relationship between phospholipids and insulin resistance: From clinical to experimental studies. *J. Cell. Mol. Med.* **23**, 702–710 (2019).

149. Swayne, L. A., Sorbara, C. D. & Bennett, S. A. L. Pannexin 2 is expressed by postnatal hippocampal neural progenitors and modulates neuronal commitment. *J. Biol. Chem.* **285**, 24977–24986 (2010).

150. Vasseur, M. Le, Chen, V. C., Huang, K., Vogl, W. A. & Naus, C. C. Pannexin 2 localizes at ER-mitochondria contact sites. *Cancers (Basel).* **11**, 1–19 (2019).

151. Dourado, M., Wong, E. & Hackos, D. H. Pannexin-1 is blocked by its C-terminus through a delocalized non-specific interaction surface. *PLoS One* **9**, (2014).

152. Bialecki, J. *et al.* Suppression of presynaptic glutamate release by postsynaptic metabotropic NMDA receptor signalling to pannexin-1. *J. Neurosci.* **40**, 729–742 (2020).

153. Weilinger, N. L. *et al.* Metabotropic NMDA receptor signaling couples Src family kinases to pannexin-1 during excitotoxicity. *Nat. Neurosci.* **19**, 432–442 (2016).

154. Seeliger, M. A. *et al.* High yield bacterial expression of active c-Abl and c-Src tyrosine kinases. *Protein Sci.* **14**, 3135–3139 (2005).

155. Nouri-Nejad, D. *et al.* Pannexin 1 mutation found in melanoma tumor reduces phosphorylation, glycosylation, and trafficking of the channel-forming protein. *Mol. Biol.*

Cell **32**, 376–390 (2021).